

# Passive Realizations of Series Elastic Actuation: Passivity and Effects of Plant and Controller Dynamics on Haptic Rendering Performance

Celal Umut Kenanoglu

Volkan Patoglu

**Abstract**—We establish the necessary and sufficient conditions for the frequency domain passivity of series (damped) elastic actuation (S(D)EA) while rendering null impedance and ideal springs under velocity sourced impedance control (VSIC). We introduce passive physical equivalents for S(D)EA under closed-loop control to help establish an intuitive understanding of the passivity bounds and to highlight the effect of different plant parameters and controller gains on the closed-loop performance of the system. Through the passive physical equivalents, we rigorously compare the effect of different plants dynamics (e.g., SEA and SDEA) and different cascaded controller architectures (e.g., P-P and P-PI) on the system performance. We show that passive physical equivalents establish a natural means for effective impedance analysis. We provide experimental validations of our theoretical results and evaluate the haptic rendering performance of S(D)EA under VSIC.

**Index Terms**—Physical Human-Robot Interaction, Interaction Control, Series Elastic Actuation, Network Synthesis, Physical Realizations, Coupled Stability, Effective Impedance.

## I. INTRODUCTION

ESTABLISHING safe and natural physical human-robot interactions (pHRI) is vital in many applications, including collaborative manufacturing, service, surgical, assistive, and rehabilitation robotics. Safe and natural pHRI necessitate precise control of the impedance characteristics of the robot at the interaction port [1], [2].

Series elastic actuation (SEA) is a commonly employed interaction control paradigm that has been introduced in [3]–[5] to address the fundamental trade-off between the stability robustness and control performance of closed-loop force control systems [6]–[8]. SEA relies on an intentionally introduced compliant element between the actuator and the interaction port, and utilizes the model of this compliant element to implement closed-loop force control. Thanks to SEA, the strict stability bounds on the controller gains induced due to sensor-actuator non-collocation and bandwidth limitations can be relaxed, leading to high stability robustness and good rendering performance. On the negative side, the introduction of the compliant element significantly decreases the system bandwidth; consequently, the control effort increases quickly for high-frequency interactions, resulting in actuator (velocity and/or torque) saturation.

Series damped elastic actuation (SDEA) extends SEA by introducing a viscous dissipation element parallel to the series

elastic element [9]–[13]. SDEA can, not only help increase the force control bandwidth of SEA [9] but also provide additional advantages, in terms of improving energy efficiency [11], reducing undesired oscillations [12], and alleviating the need for derivative control terms [13].

Coupled stability of interactions with S(D)EA have commonly been studied through the frequency domain passivity analysis. Given that inanimate environments are passive and non-malicious human interactions do not intentionally aim to destabilize a system, the frequency domain passivity analysis can be utilized to conclude coupled stability of interactions [2]. While frequency domain passivity is known to be conservative, closed-form analytical passivity conditions derived through such analysis are informative, as they provide insights on how system parameters affect stability robustness.

**Contributions:** In this paper, we rigorously study the passivity of S(D)EA to establish closed-form analytical solutions for the necessary and sufficient conditions for frequency domain passivity of S(D)EA while rendering ideal springs and null impedance. Our results extend the previously established bounds in the literature, as we allow for the negative selection of the controller gains. More importantly, we propose *passive physical equivalents* as a novel and informative means of providing physical insight to the passivity conditions and derive such passive physical equivalents for S(D)EA under closed-loop control. We advocate that passive physical equivalents can be instrumental, as they

- provide sufficient conditions for the passivity,
- establish an intuitive understanding of the passivity bounds, explicitly highlighting the effect of different plant parameters and controller gains on the closed-loop rendering performance,
- do not distinguish between the plant and controller parameters, promoting co-design of S(D)EA by enforcing simultaneous and unbiased consideration of these (possibly negative) parameters on the system performance,
- subsume the effective impedance analysis that decomposes the output impedance into its basic mechanical primitives and extend it by providing a topological connection of these fundamental elements, and
- enable rigorous and intuitive comparisons of the effect of different plants dynamics (e.g., SEA and SDEA) and controller architectures (e.g., P-P and P-PI) on the haptic rendering performance.

C. U. Kenanoglu and V. Patoglu are with the Faculty of Engineering and Natural Sciences at Sabancı University, İstanbul, Turkey. E-mail: {umut.kenanoglu,volkan.patoglu}@sabanciuniv.edu

## II. RELATED WORK

In this section, we discuss the related works on frequency domain passivity of S(D)EA, and review the classical results and recent developments in the realization of passive networks.

### A. Frequency Domain Passivity of SEA

To the best of authors' knowledge, Pratt *et al.* have presented the first passivity analysis for SEA, and provided sufficient conditions for a SEA under a filtered PID force controller with a feedforward compensator [4]. Since the introduction of velocity-sourced impedance control (VSIC) for SEA [3], [14]–[16], passivity of SEA under VSIC has been studied extensively [17]–[21]. VSIC has become the most popular force controller for SEA, as its cascaded control architecture with an inner motion control loop can effectively eliminate parasitic forces, leading to good rendering performance [3], [5], [16], [22]. Furthermore, VSIC is easy-to-use, since this controller does not rely on the dynamic model of the plant and the controller gains can be empirically tuned.

Vallery *et al.* have provided a set of sufficient conditions for null impedance and ideal spring rendering with SEA under VSIC [17], [18]. They have also proved that the passively renderable stiffness of a SEA under VSIC is upper bounded by the physical stiffness of the compliant element of SEA [18]. Tagliamonte *et al.* have provided less conservative sufficient conditions for passivity of SEA under VSIC during null impedance, linear stiffness, and Maxwell body rendering [19]. They have also proved that Voigt model cannot be passively rendered with SEA under VSIC and shown that the maximum renderable stiffness not only depends on the physical stiffness, but also the physical damping in the system. Calanca *et al.* have presented sufficient conditions for passivity of SEA under four different control architectures: VSIC, basic impedance, collocated admittance, and collocated impedance controllers [20]. They have shown that passively renderable virtual stiffness of all of these control architectures are also limited by the physical stiffness of the compliant element. They have also demonstrated that Voigt model cannot be rendered passively with SEA under VSIC [20].

Tosun and Patoglu [21] have presented the necessary and sufficient conditions for the passivity of SEA under VSIC for null impedance and linear spring rendering. The earlier sufficiency bounds on controller gains have been relaxed and the range of impedances that can be passively rendered has been extended in this study. Furthermore, it has been shown that integral gain of the motion controller is required to render stiffness if the force controller utilizes an integral term.

Recently, authors have proposed the use of model reference force control (MRFC) for SEA and provided passivity analysis of this control scheme, under model mismatch. In particular, sufficient conditions for passivity of SEA under MRFC during null impedance rendering have been presented in [23].

### B. Frequency Domain Passivity of SDEA

SDEA generalizes SEA by introducing a viscous dissipation element parallel to the series elastic element. Accordingly,

the passivity analysis of SDEA also generalizes the passivity analysis of SEA, as most SEA results can be recovered as the effect of the dissipation element approaches to zero. However, passivity analysis of SDEA has received relatively less attention in the literature, since the resulting closed-form solutions are more complex and much harder to interpret [10], [24]–[26].

The passive range of virtual stiffness and damping parameters for SDEA under a cascaded impedance controller with an inner torque loop acting on a velocity compensated plant and load dynamics have been studied in [24]. In this controller, a positive velocity feedback loop provides velocity compensation by attempting to extend the bandwidth of the torque control loop under the passivity constraints.

Oblak and Matjacic [10] have conducted a frequency domain passivity analysis of SDEA under an unconventional basic impedance controller. In this controller, a force sensor is employed after the end-effector inertia to measure the interaction forces, and these forces are used for closed-loop force control, in addition to the series damped elastic element. It has been demonstrated that a sufficient level of mechanical damping is required in the compliant element to ensure the passivity of linear stiffness rendering using this control architecture. Furthermore, sufficient conditions to passively render linear springs have been proposed, which include a lower bound on the required level of physical damping.

Recently, Mengilli *et al.* have presented the sufficient conditions for the passivity of SDEA under VSIC for the null impedance, pure spring, and Voigt model rendering [26]. Furthermore, they have extended these results to absolute stability and two-port passivity analysis and derived the necessary and sufficient conditions for a virtual coupler [25].

### C. Realization of Passive Physical Equivalents

Passive physical equivalents are studied in the field of network synthesis, which aim to rigorously describe physically realizable behaviours in a given domain with specified components. In particular, the goal in network synthesis is to design a passive network of fundamental elements to realize a given driving-point impedance.

Colgate and Hogan have advocated the use of passive physical equivalents for the analysis of contact instability observed in interaction control. Through passive realizations of force controlled systems, they have shown a fundamental limitation on inertia cancellation under passivity constraints for force-feedback systems with sensor-actuator non-collocation [27].

Similar to [27], this paper also focuses on linear passive mechanical networks, built utilizing springs, dampers, and inerters—a relatively recently introduced fundamental element of the mechanical domain [28], [29]. Inerter element completes the force-current analogy between the electrical and mechanical domains by introducing an ideal linear two-terminal energy storage element equivalent to an ungrounded capacitor. The completion of the analogy has a major impact, as it enables all of the previously established results in the electrical network synthesis to be equivalently expressed in the mechanical

domain. Thanks to this analogy, all classical results, including Foster’s reactance theorem [30] characterizing lossless networks, Brune’s construction method [31] for the realization of general positive-real functions using resistors, inductors, capacitors, and transformers, and Bott-Duffin theorem [32] indicating transformers are not necessary in the synthesis of positive-real impedances, can be directly used for the network synthesis in the mechanical domain.

While network synthesis in the electrical domain has received much attention during the era of analog circuits, the diminished attention has been renewed during the last decade, especially in the mechanical domain, with the introduction of inerter element and demonstration of its successful applications in the design of passive suspensions [28], [33]–[38].

Kalman has also advocated for a renewed focus on the network synthesis to establish a general theory of the subject, pointing out the high potential of this field to have wide impact in a broad range of applications [39]. Accordingly, recent results have been established to extend the classical ones. Chen and Smith have studied the most general class of mechanical impedances that can be realized using one damper, one inerter, and an arbitrary number of spring elements, while allowing no levers [34]. Jiang and Smith have studied the realizability conditions for positive-real biquadratic impedance functions which can be realized by five-element [40] and six-element [41] networks. Chen *et al.* have extended their earlier results in [36] and established the realizability conditions to two special class of mechanical networks: networks with biquadratic functions with an extra pole at the origin [37] and networks that are constituted of one inerter, one damper, and at most three springs [38]. Hughes and Smith have extended the classical results on Bott–Duffin realization procedure by discussing the minimality and uniqueness of these realizations among all series-parallel networks realizing biquadratic minimum functions [42]. Hughes has further extended these results and established minimal network realizations for the class of impedances realized by series-parallel networks containing at most three energy storage elements [43], [44]. Morelli and Smith have presented an enumerative approach to the passive network synthesis and provided a classification for networks of restricted complexity [45]. Readers are referred to the survey by Hughes *et al.* for a review of the recent developments [46].

#### D. Rendering Performance

While the coupled stability of pHRI systems constitutes an imperative design criterion, the rendering performance of the

system is also significant for natural interactions. Transparency is a commonly used concept in evaluation of the haptic rendering performance, as it quantifies the match between the mechanical impedance of the virtual environment and the impedance felt by the user, with the requirement of identical force/velocity responses [47], [48].  $Z_{width}$  is another commonly used metric that quantifies the difference between the minimum and the maximum passively renderable impedances [49].

Given that the rendered impedance is a function of frequency, both of these metrics are also quantified as such; however, the frequency dependence of these metrics make their interpretation challenging. To provide physical intuition to the characteristics of the impedance at the interaction port, it is common practice to decompose the impedance into its basic *mechanical primitives* through effective impedance analysis [50]–[55]. In particular, effective impedance definitions partition the frequency dependent impedance transfer function into its real and imaginary parts, assign the real positive part to effective damping, while imaginary part is mapped to effective spring and effective mass components based on the phase response of the impedance.

While the effective impedance analysis is quite useful, the use of passive physical equivalents extends this concept, since a feasible realization also provides a topological connection of the fundamental mechanical elements. Along these lines, passive physical equivalents subsume the effective impedance analysis, and provide a more intuitive understanding of system behaviour and its underlying components.

### III. PRELIMINARIES

In this section, we present the LTI model of SDEA under VSIC (Figure 1) and review the relevant theorems used to study the frequency domain passivity of LTI systems.

#### A. System Description

Figure 2 depicts a schematic representation of a single degree of freedom SDEA plant without its controller. The reflected inertia of the actuator is denoted by  $J_m$ , the viscous friction of the actuator including the reflected motor damping is denoted by  $B_m$ , the physical compliant element and viscous damper, arranged in parallel between the end-effector and the actuator, are denoted by  $K$  and  $B_f$ , respectively. Symbols  $\omega_m$  and  $\omega_{end}$  denote the actuator and end-effector velocities, respectively. The actuator torque is shown with  $\tau_m$ .

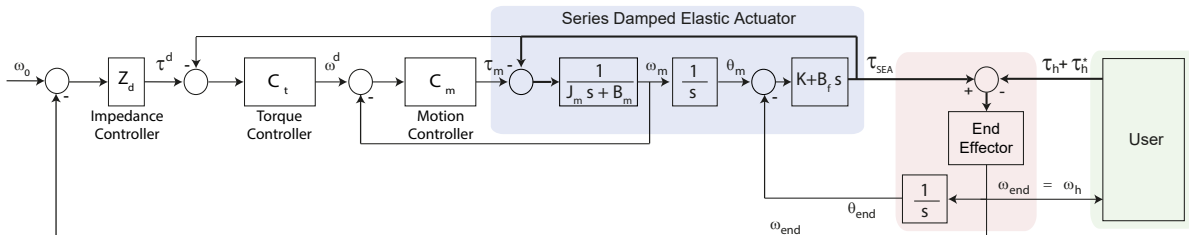


Fig. 1: Block diagram of S(D)EA under VSIC

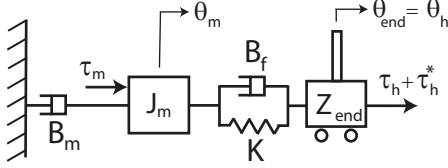


Fig. 2: Schematic representation of SDEA (The plant reduces to an SEA when  $B_f = 0$ .)

The torque  $\tau_{sea}$  on the damped compliant element, also called the physical filter, is equal to the sum of the torques induced on the linear spring and the viscous damper elements. Figure 2 represents a SEA, when  $B_f$  is set to zero. In this case,  $\tau_{sea}$  can be computed using the deflections of the linear spring  $K$ , according to the Hooke's law.

Human interaction is modeled with two components:  $\tau_h$  represents the passive component of the applied torques while  $\tau_h^*$  is the deliberately applied active component that is assumed to be independent of system states [2]. We assume that the non-malicious human interactions do not intentionally aim to destabilize the system.

It is considered that the end-effector inertia of SDEA is negligible or is a part of the user dynamics such that  $\tau_{sea}(s) \approx \tau_h + \tau_h^*$ ; hence, the impedance at the human/environment interaction port can be defined as  $Z_{out}(s) = -\frac{\tau_{sea}(s)}{\omega_{end}(s)}$ , where the spring-damper torque is considered as positive when these elements are in compression.

Figure 1 depicts the block diagram of SDEA under VSIC, where thick lines present physical forces. In this cascaded controller, the inner velocity control loop of the cascaded controller renders the system into an ideal motion source and acts on references generated by the outer torque control loop to keep the spring-damper deflection at the desired level to match the reference force for SDEA.  $C_t$  and  $C_m$  denote the torque and motion (velocity) controllers, respectively.

The following assumptions are considered for the analysis:

- A linear time-invariant (LTI) model is considered. Therefore, nonlinear effects, such as backlash, stiction, and actuator saturation are neglected.
- Electrical dynamics are neglected and actuator velocity is assumed to be available with a negligible time delay.
- Both the deflection induced on the physical filter and its time derivative are assumed to be measured with a negligible time delay.
- Without loss of generality, a zero motion reference ( $\omega_d=0$ ) is assumed for the virtual environment and the transmission ratio is set to one for simplicity of analysis.
- The physical plant parameters are assumed to be positive, while the controller gains are allowed to be negative.

### B. Passivity Theorems

Passivity of an LTI network in the frequency domain is equivalent to the positive realness of its impedance transfer function  $Z(s)$  [56]. The positive realness of a rational function  $Z(s)$  with real coefficients can be studied according to Theorem 1 as follows.

**Theorem 1** ([2], [57], [58]). A rational impedance transfer function  $Z(s)$  with real coefficients is passive if and only if: (1)  $Z(s)$  has no poles in the right half plane, and (2)  $\text{Re}[Z(j\omega)] \geq 0$  for all  $\omega$ , and (3) Any poles of  $Z(s)$  on the imaginary axis are simple with positive and real residues.

Following useful lemmas have been established in the literature to determine the necessary and sufficient conditions for the frequency domain passivity of LTI systems.

**Lemma 1.** Let  $Z(s) = N(s)/D(s)$  be an impedance transfer function. Then,  $\text{Re}[Z(j\omega)] \geq 0$  if and only if  $P(\omega) \geq 0$  for any value of  $\omega$ , where  $P(\omega) = \text{Re}[N(j\omega)D(-j\omega)] = \sum_{i=0}^n d_i \omega^i$ , where  $d_i$  represents the coefficient of  $\omega^i$ .

**Lemma 2.** Let  $f(s) = a_3 s^3 + a_2 s^2 + a_1 s + a_0$  for  $a_i \geq 0$  be the third-order characteristic equation of a system. Then,  $f(s)$  has no roots in the open right half plane if and only if  $a_3 \geq 0$ ,  $a_2 \geq 0$ ,  $a_0 \geq 0$ , and  $a_1 a_2 - a_0 a_3 \geq 0$ . If these inequalities are strictly greater than zero, then the system has no roots on the imaginary axis.

**Lemma 3** ([25]). A polynomial of the form  $p(x) = p_2 x^2 + p_1 x + p_0$ ,  $p(x) \geq 0$  for all  $x \geq 0$  if and only if  $p_2 \geq 0$ ,  $p_0 \geq 0$  and  $p_1 \geq -2\sqrt{p_0 p_2}$ .

### C. Force-Current Analogy and Inerter

In the force-current analogy between the mechanical and electrical domains, forces are considered to be analogous to currents, while velocities are analogous to voltages. Accordingly, Figure 3 presents the force-current analogy between fundamental two-terminal elements in both domains.

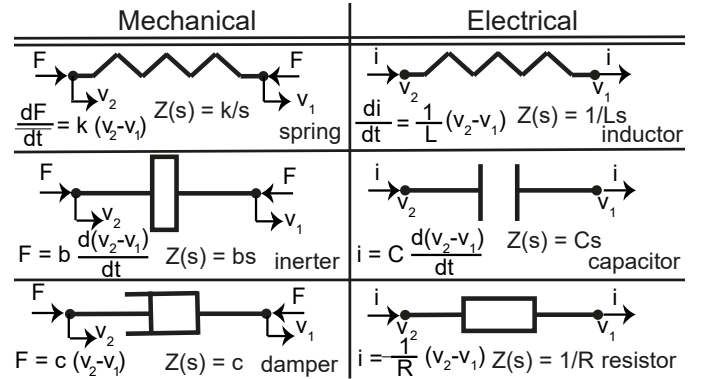


Fig. 3: Force-current analogy between the fundamental two-terminal elements in the electrical and mechanical domains.

Inerter is a relatively recently introduced ideal energy storage element that completes the force-current analogy between the mechanical and electrical domains [28], [29]. Particularly, inerter is an ideal linear two-terminal energy storage element in the mechanical domain that is equivalent to an ungrounded capacitor in the electrical domain. Inerter element generalizes the more familiar mass/inertia element in the mechanical domain, which is analogous to the restricted case of a grounded capacitor in the electrical domain.

#### IV. PASSIVITY AND PHYSICAL EQUIVALENTS OF SEA

In this section, we present the necessary and sufficient conditions for frequency domain passivity of SEA under VSIC (with P and PI controllers) while rendering null impedance and linear springs without imposing non-negativity assumption on the controller gains. The first row of Figure 4 presents a summary of passive physical equivalents for SEA under VSIC with different types of controllers.

##### A. Null Impedance Rendering

a) *When the torque and the motion controllers are taken as proportional (P) controllers:* the impedance at the interaction port of SEA under VSIC during null impedance rendering is

$$Z_{null}^{SEA^{P-P}}(s) = \frac{J_m K s + (B_m + G_m) K}{J_m s^2 + (B_m + G_m) s + (1 + \alpha) K} \quad (1)$$

where  $\alpha = G_m G_t$ .

The passivity of  $Z_{null}^{SEA^{P-P}}(s)$  is checked according to Theorem 1. Theorem 2 presents the necessary and sufficient conditions for one-port passivity of SEA under VSIC while rendering null impedance.

**Theorem 2.** *Consider null impedance rendering for SEA under VSIC as in Figure 1 with  $B_f = 0$ , where the torque and velocity controllers consist of proportional gains  $G_t$  and  $G_m$ , respectively. Let the physical plant parameters be positive, while the controller gains are allowed to be negative. Then, the following expressions constitute the necessary and sufficient conditions for the passivity of  $Z_{null}^{SEA^{P-P}}(s)$ :*

- (i)  $(B_m + G_m) \geq 0$ , and
- (ii)  $\alpha + 1 \geq 0$ .

*Proof:* 1)  $Z(s)$  has no poles in the right half plane. If we apply the Routh-Hurwitz stability criterion,  $Z_{null}^{SEA^{P-P}}(s)$  has no roots in the open right half plane if  $(B_m + G_m)$  and  $(\alpha + 1)$  are non-negative.

2)  $Re[Z(jw)] \geq 0$  for all  $w$ . Invoking Lemma 1, the sign of  $Re[Z_{null}^{SEA^{P-P}}(jw)]$  can be checked by the sign of  $H(jw) = K^2(\alpha + 1)(B_m + G_m)$ .  $Re[Z_{null}^{SEA^{P-P}}]$  is guaranteed to be non-negative if  $(B_m + G_m)$  and  $(\alpha + 1)$  are non-negative.

3) Any poles of  $Z(s)$  on the imaginary axis are simple with positive and real residues. There exists no poles on imaginary axis if  $(\alpha + 1)$  and  $(B_m + G_m)$  are positive. Given that plant parameters  $J_m$  and  $K$  are positive, Eqn. (1) is passive when  $(\alpha + 1) = 0$ , since Eqn. (1) equals to  $\frac{K}{s}$ , which models a passive physical spring. A special case occurs when  $(B_m + G_m) = 0$ , for which there exist simple poles on the imaginary axis. The residues of these imaginary poles equal to  $\frac{J_m K}{2}$ , which is positive. ■

**Passive Physical Equivalent:** A realization of Eqn. (1) characterizing SEA under VSIC during null impedance rendering when both controllers are P is presented in Figure 4b.

For the realization in Figure 4b to be feasible, all physical components in the model should be non-negative, that is,

$(B_m + G_m)$  and  $(\alpha + 1)$  should be non-negative, given the plant parameters  $J_m$ ,  $B_m$ , and  $K$  are positive. In the special case when  $(\alpha + 1) = 0$ , the damper and inerter elements converge to infinity and the system behaves as a pure spring.

**Feasibility of Passive Realization vs Passivity:** The conditions for the feasibility of the realization in Figure 4b are equivalent to the necessary and sufficient conditions for the passivity of Eqn. (1) according to Theorem 1: if the  $(B_m + G_m) \geq 0$  and  $(\alpha + 1) \geq 0$ , then Eqn. (1) is passive and all components in Figure 4b are non-negative.

b) *When the torque controller is taken as proportional (P) and the motion controller is taken as proportional-integral (PI) controller:* the impedance at the interaction port of SEA under VSIC during null impedance rendering equals to

$$Z_{null}^{SEA^{P-PI}}(s) = \frac{J_m K s^2 + (B_m + G_m) K s + I_m K}{J_m s^3 + (B_m + G_m) s^2 + (I_m + (1 + \alpha) K) s + G_t I_m K} \quad (2)$$

where  $\alpha = G_m G_t$ . The passivity of  $Z_{null}^{SEA^{P-PI}}(s)$  is checked according to Theorem 1. Theorem 3 presents the necessary and sufficient conditions for one-port passivity of SEA under VSIC while rendering null impedance, when the torque controller is taken as proportional (P) and the motion controller is taken as proportional-integral (PI) controller.

**Theorem 3.** *Consider null impedance rendering for SEA under VSIC as in Figure 1 with  $B_f = 0$ , where the torque controller consists of a proportional gain  $G_t$ , while the velocity controller consists of proportional-integral gains  $G_m$  and  $I_m$ , respectively. Let the physical plant parameters be positive, while the controller gains are allowed to be negative. Then, the following expressions constitute the necessary and sufficient conditions for the passivity of  $Z_{null}^{SEA^{P-PI}}(s)$ :*

- (i)  $J_m \leq \frac{(\alpha+1)(B_m+G_m)}{G_t I_m}$ , and
- (ii)  $\alpha + 1 > 0$ , and
- (iii)  $B_m + G_m > 0$ , and
- (iv)  $G_t \geq 0$ , and
- (v)  $I_m \geq 0$ .

*Proof:* 1)  $Z(s)$  has no poles in the right half plane. If we apply the Routh-Hurwitz stability criterion,  $Z_{null}^{SEA^{P-PI}}(s)$  has no roots in the open right half plane if  $(B_m + G_m)$  and  $G_t I_m$  are non-negative and the following condition is satisfied.

$$J_m \leq \frac{(B_m + G_m)(I_m + (1 + \alpha) K)}{G_t I_m K} \quad (3)$$

2)  $Re[Z(jw)] \geq 0$  for all  $w$ . Invoking Lemma 1, the sign of  $Re[Z_{null}^{SEA^{P-PI}}(jw)]$  can be checked by the sign of  $H(jw) = d_2 w^2 + d_0$  where

$$d_0 = G_t I_m^2 K^2 \quad (4)$$

$$d_2 = -G_t I_m K^2 J_m + K^2 (B_m + G_m)(\alpha + 1) \quad (5)$$

$Re[Z_{null}^{SEA^{P-PI}}]$  is non-negative if  $G_t \geq 0$  as required for the non-negativeness of  $d_0$ , and  $(\alpha + 1) > 0$ ,  $(B_m + G_m) > 0$  and Eqn. (6) holds as required for the non-negativeness of  $d_2$ .

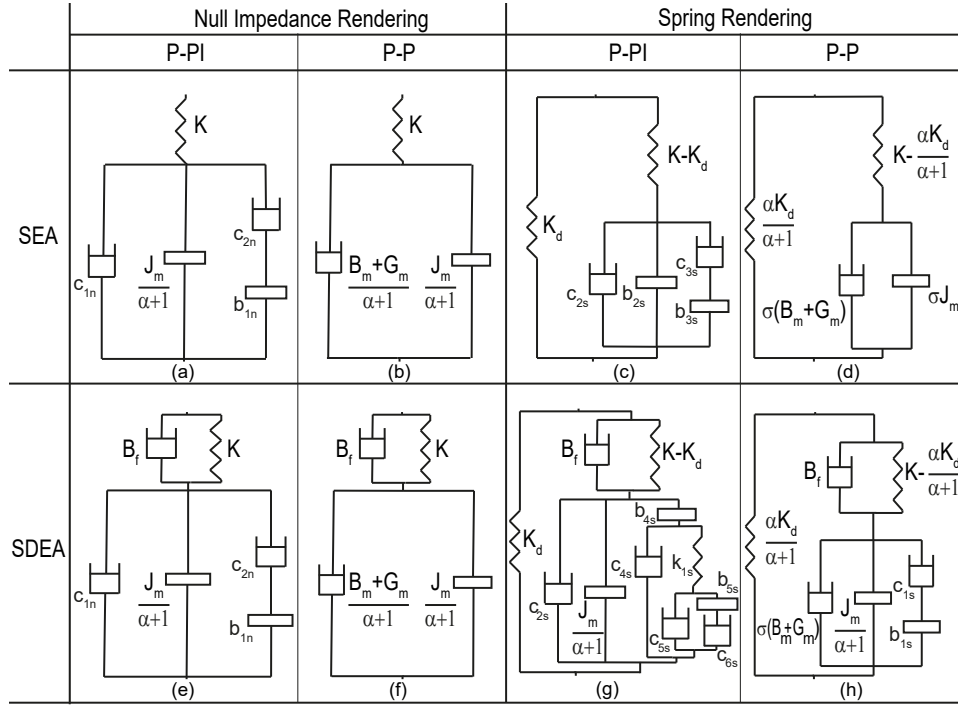


Fig. 4: Passive physical equivalents for SEA and SDEA under VSIC with different types of controller

Note that if Eqn. (6) holds, then Eqn. (3) is also guaranteed to hold.

$$J_m \leq \frac{(\alpha + 1)(B_m + G_m)}{G_t I_m} \quad (6)$$

3) Any poles of  $Z(s)$  on the imaginary axis are simple with positive and real residues. No roots exist on the imaginary axis if  $(B_m + G_m)$  and  $G_t I_m$  are positive. For the special case when  $G_t = 0$ , there is a simple pole on the imaginary axis whose residue is  $\frac{J_m K}{I_m + K}$ . Note that,  $G_t \geq 0$  and  $G_t I_m \geq 0$  imply that  $I_m \geq 0$ . When  $I_m = 0$ , Eqn. (2) reduces to Eqn. (1) as analysed in the previous subsection. ■

**Passive Physical Equivalent:** A realization of Eqn. (2) characterizing SEA under VSIC during null impedance rendering when the motion controller is PI and the torque controller is P is presented in Figure 4a, where  $c_{1n} = \frac{1}{G_t}$ ,  $c_{2n} = \frac{B_m - \frac{1}{G_t}}{\alpha + 1} - \frac{G_t I_m J_m}{(\alpha + 1)^2}$ , and  $b_{1n} = \frac{B_m G_t - 1}{G_t^2 I_m} - \frac{J_m}{\alpha + 1}$ .

For the realization in Figure 4a to be feasible, all physical components in the model should be non-negative. Therefore,  $(\alpha + 1)$  should be non-negative from the inerter term, while  $G_t$  should be non-negative for a non-negative  $c_{1n}$ . The non-negativeness of  $b_{1n}$  imposes

$$J_m \leq \frac{(\alpha + 1)(B_m G_t - 1)}{G_t^2 I_m} \quad (7)$$

If  $I_m \geq 0$ , then Eqn. (7) ensures the non-negativeness of  $c_{2n}$ , while also indicating that  $(B_m G_t - 1)$  and  $(\alpha + 1)$  should be positive. It is not possible to select  $I_m < 0$ , as the non-negativeness of  $c_{2n}$  conflicts with Eqn. (7) in this case.

**Feasibility of Passive Realization vs Passivity:** Given  $(\alpha + 1) > 0$  as necessitated by the feasibility of the realization in Figure 4a and the passivity of Eqn. (2), Eqns. (6) and (7)

can be expressed together as

$$\frac{J_m}{(\alpha + 1)} \leq \frac{(B_m G_t - 1)}{G_t^2 I_m} < \frac{(B_m + G_m)}{G_t I_m} \quad (8)$$

Consequently, Eqn. (7) presents a more conservative bound and its satisfaction ensures that Eqn. (6) is also satisfied. Lastly, it can be shown that when  $(B_m G_t - 1) > 0$  is summed with  $(\alpha + 1) > 0$ , the result is equivalent to  $(B_m + G_m) > 0$ , which is known to be positive, since  $G_t > \frac{1}{B_m}$ .

Hence, the conditions for the feasibility of the realization in Figure 4a provide sufficient conditions for the passivity of Eqn. (2) according to Theorem 1. In particular, Eqn. (7) implies Eqn. (6) if  $(\alpha + 1) > 0$ , as necessitated by the non-negativeness of  $c_{2n}$  term. Furthermore, the condition  $(B_m G_t - 1) > 0$  imposed by the non-negativeness of  $c_{2n}$  implies  $(B_m + G_m) > 0$ , when considered with  $(\alpha + 1) > 0$ .

To summarize, the realization in Figure 4a is feasible and the sufficient conditions for the passivity of Eqn. (2) are satisfied if  $(B_m G_t - 1)$  and  $(\alpha + 1)$  are positive,  $I_m$  is non-negative, and Eqn. (7) is satisfied. The necessary and sufficient conditions for the passivity of Eqn. (2) can be enforced if Eqn. (6) is imposed instead of Eqn. (7), and  $G_t \geq 0$  and  $(B_m + G_m) > 0$  are imposed instead of  $(B_m G_t - 1) > 0$ .

### B. Spring Rendering

When both the motion and torque controllers are taken as proportional (P) controllers, the impedance at the interaction port of SEA under VSIC during spring rendering equals to

$$Z_{spring}^{SEA^{P-P}}(s) = \frac{J_m K s^2 + (B_m + G_m) K s + \alpha K K_d}{J_m s^3 + (B_m + G_m) s^2 + (\alpha + 1) K s} \quad (9)$$

where  $\alpha = G_m G_t$ . Note that when  $(\alpha + 1) = 0$ , the rendering of virtual springs is no longer possible.

The passivity of  $Z_{spring}^{SEA^{P-P}}(s)$  is checked according to Theorem 1. Theorem 4 presents the necessary and sufficient conditions for the passivity of SEA under VSIC while rendering springs.

**Theorem 4.** *Consider spring rendering for SEA under VSIC as in Figure 1 with  $B_f = 0$ , where the torque and velocity controllers consist of proportional gains  $G_t$  and  $G_m$ , respectively. Let the physical plant parameters be positive, while the controller gains are allowed to be negative. Then, the following expressions constitute the necessary and sufficient conditions for the passivity of  $Z_{spring}^{SEA^{P-P}}(s)$ :*

- (i)  $K \geq \frac{\alpha}{\alpha+1} K_d$ , and
- (ii)  $\frac{\alpha}{\alpha+1} K_d > 0$ , and
- (iii)  $\alpha + 1 > 0$ , and
- (iv)  $(B_m + G_m) \geq 0$ .

*Proof:* 1)  $Z(s)$  has no poles in the right half plane. If we apply the Routh-Hurwitz stability criterion,  $Z_{spring}^{SEA^{P-P}}(s)$  has no roots in the open right half plane, if  $(B_m + G_m)$  and  $(\alpha + 1)$  are non-negative.

2)  $Re[Z(jw)] \geq 0$  for all  $w$ . Invoking Lemma 1, the sign of  $Re[Z_{spring}^{SEA^{P-P}}(jw)]$  can be checked by the sign of  $H(jw) = d_2 w^2$ , where  $d_2 = K^2(\alpha + 1)(B_m + G_m) - \alpha K K_d(B_m + G_m)$ . Here,  $d_2$  is guaranteed to be non-negative if

$$K \geq \frac{\alpha}{\alpha+1} K_d \quad (10)$$

Note that, if  $G_m$  is negative,  $G_t$  should also be negative to ensure that  $\frac{\alpha}{\alpha+1} K_d$  is positive.

3) Any poles of  $Z(s)$  on the imaginary axis are simple with positive and real residues. If  $(B_m + G_m)$  and  $(\alpha + 1)$  are positive, then the only possible root on the imaginary axis is at zero with a residue of  $\frac{\alpha}{\alpha+1} K_d$ . For the special case, when  $(B_m + G_m) = 0$ , there exists simple poles on the imaginary axis whose residues are  $\frac{J_m(K-K_d)}{2} - \frac{J_m K_d}{2 B_m G_t - 2}$ . This residue is positive if Eqn. (10) is satisfied. Note that, when  $(\alpha + 1) = 0$ , the output impedance transfer function becomes equal to  $\frac{(J_m K) s^2 + (B_m + G_m) K s - K K_d}{J_m s^3 + (B_m + G_m) s^2}$  and Condition 3 of Theorem 1 is violated as double poles exist at  $s = 0$ . ■

Passive Physical Equivalent: A realization of Eqn. (9) characterizing SEA under VSIC during spring rendering when both controllers are proportional is presented in Figure 4d, where  $\sigma = \frac{1}{\alpha+1} - \frac{\alpha}{(\alpha+1)^2} \frac{K_d}{K}$ .

For the realization in Figure 4d to be physically feasible, all of components of the model should be non-negative. All components in the realization are guaranteed to be non-negative, if  $(B_m + G_m)$  is non-negative, and  $\frac{\alpha}{\alpha+1} K_d$  and  $(\alpha + 1)$  are positive.

Feasibility of Passive Realization vs Passivity: The conditions for the feasibility of the realization in Figure 4d are equivalent to the necessary and sufficient conditions for passivity of Eqn. (9) according to Theorem 1: if  $(B_m + G_m)$  is non-negative, and  $(\alpha + 1)$  and  $\frac{\alpha}{\alpha+1} K_d$  are positive, then Eqn. (9) is passive and all components in Figure 4d are non-negative.

## V. PASSIVITY AND PHYSICAL EQUIVALENTS OF SDEA

In this section, we present the necessary and sufficient conditions for the frequency domain passivity of SDEA under VSIC with P controllers, while rendering null impedance and linear springs without imposing non-negativity assumption on the controller gains. The second row of Figure 4 presents a summary of passive physical equivalents for SDEA under VSIC with different types of controllers.

### A. Null Impedance Rendering

When the torque and the motion controllers are taken as proportional (P) controllers, the impedance at the interaction port of SDEA under VSIC during null impedance rendering equals to

$$Z_{null}^{SDEA^{P-P}}(s) = \frac{B_f J_m s^2 + (B_f (B_m + G_m) + J_m K) s + K(B_m + G_m)}{J_m s^2 + (B_f (1 + \alpha) + B_m + G_m) s + K(\alpha + 1)} \quad (11)$$

where  $\alpha = G_m G_t$ . Note that when  $(\alpha + 1) = 0$ , Eqn. (11) equals to  $B_f + \frac{K}{s}$ , which is passive.

The passivity of  $Z_{null}^{SDEA^{P-P}}(s)$  is checked according to Theorem 1. Theorem 5 presents the necessary and sufficient conditions for the passivity of SDEA under VSIC while rendering null impedance.

**Theorem 5.** *Consider null impedance rendering for SDEA under VSIC as in Figure 1, where the torque and velocity controllers consist of proportional gains  $G_t$  and  $G_m$ , respectively. Let the physical plant parameters be positive, while the controller gains are allowed to be negative. Then, the following expressions constitute the necessary and sufficient conditions for the passivity of  $Z_{null}^{SDEA^{P-P}}(s)$ :*

- (i)  $(B_m + G_m) \geq 0$ , and
- (ii)  $\alpha + 1 \geq 0$ .

*Proof:* 1)  $Z(s)$  has no poles in the right half plane. If we apply the Routh-Hurwitz stability criterion,  $Z_{null}^{SDEA^{P-P}}(s)$  has no poles in the right half plane if  $B_m + G_m + B_f(\alpha + 1)$  and  $(\alpha + 1)$  are non-negative.

2)  $Re[Z(jw)] \geq 0$  for all  $w$ . Invoking Lemma 1, the sign of  $Re[Z_{null}^{SDEA^{P-P}}(jw)]$  can be checked by the sign of  $H(jw) = d_4 w^4 + d_2 w^2 + d_0$  where

$$d_0 = K^2 (\alpha + 1) (B_m + G_m) \quad (12)$$

$$d_2 = B_f (B_m + G_m) (B_m + G_m + B_f(\alpha + 1)) \quad (13)$$

$$d_4 = B_f J_m^2 \quad (14)$$

$Re[Z_{null}^{SDEA^{P-P}}]$  is non-negative if  $B_m + G_m + B_f(\alpha + 1)$ ,  $(\alpha + 1)$ , and  $(B_m + G_m)$  are non-negative.

3) Any poles of  $Z(s)$  on the imaginary axis are simple with positive and real residues. When  $B_m + G_m + B_f(\alpha + 1)$  and  $(\alpha + 1)$  are positive, this condition is satisfied. For the special case, when  $(\alpha + 1) = 0$ , Eqn. (11) reduces to  $B_f + \frac{K}{s}$ , which is always passive. There exists a pole on the imaginary axis when  $B_m + G_m + B_f(\alpha + 1) = 0$ . However,  $B_m + G_m + B_f(\alpha + 1) = 0$ , if and only if  $(\alpha + 1) = 0$ , since  $(B_m + G_m) \geq 0$  and  $(\alpha + 1) \geq 0$ . ■

Passive Physical Equivalent: A realization of Eqn. (11) characterizing SDEA under VSIC during null impedance rendering when both controllers are proportional is presented in Figure 4f.

For the realization in Figure 4f to be feasible, all physical components in the model should be non-negative, that is,  $(B_m + G_m)$  and  $(\alpha + 1)$  should be non-negative.

Feasibility of Passive Realization vs Passivity: The conditions for the feasibility of the realization in Figure 4f are equivalent to the necessary and sufficient conditions for the passivity of Eqn. (11) according to Theorem 1: if  $(B_m + G_m) \geq 0$  and  $(\alpha + 1) \geq 0$ , then Eqn. (11) is passive and all components in Figure 4f are non-negative.

### B. Spring Rendering

When the torque and the motion controllers taken as proportional (P) controllers, the impedance at the interaction port of SDEA under VSIC during spring rendering equals to

$$Z_{spring}^{SDEA^{P-P}}(s) = \frac{B_f J_m s^3 + (B_f (B_m + G_m) + J_m K) s^2 + (K (B_m + G_m) + B_f K_d \alpha) s + K K_d \alpha}{J_m s^3 + (B_f (1 + \alpha) + B_m + G_m) s^2 + K (\alpha + 1) s} \quad (15)$$

where  $\alpha = G_m G_t$ . The passivity of  $Z_{spring}^{SDEA^{P-P}}(s)$  is checked according to Theorem 1. Theorem 6 presents the necessary and sufficient conditions for the passivity of SDEA under VSIC while rendering ideal springs.

**Theorem 6.** Consider spring rendering for SDEA under VSIC as in Figure 1, where the torque and velocity controllers consist of proportional gains  $G_t$  and  $G_m$ , respectively. Let the physical plant parameters be positive, while the controller gains are allowed to be negative. Then, the following expressions constitute the necessary and sufficient conditions for the passivity of  $Z_{spring}^{SDEA^{P-P}}(s)$ :

- (i)  $K \geq \frac{\alpha}{\alpha+1} K_d$ , and
- (ii)  $\frac{\alpha}{\alpha+1} K_d > 0$ , and
- (iii)  $\alpha + 1 > 0$ , and
- (iv)  $(B_m + G_m) > 0$ , and
- (v)  $-2 J_m \sqrt{B_f K (B_m + G_m) (K + \alpha (K - K_d))} \leq B_f ((B_m + G_m) (B_f (1 + \alpha) + B_m + G_m) - \alpha J_m K_d)$ .

*Proof:* 1)  $Z(s)$  has no poles in the right half plane. Invoking Lemma 2 imposes  $(\alpha + 1) (B_m + G_m + B_f (\alpha + 1)) \geq 0$ . Accordingly,  $Z_{spring}^{SDEA^{P-P}}(s)$  has no roots in the open right half plane, if  $(\alpha + 1)$  and  $B_m + G_m + B_f (\alpha + 1)$  are non-negative.

2)  $Re[Z(jw)] \geq 0$  for all  $w$ . Invoking Lemma 1, the sign of  $Re[Z_{spring}^{SDEA^{P-P}}(jw)]$  can be checked by the sign of  $H(jw) = d_6 w^6 + d_4 w^4 + d_2 w^2$  where

$$d_2 = K (B_m + G_m) (K (\alpha + 1) - \alpha K_d) \quad (16)$$

$$d_4 = B_f ((B_m + G_m) (B_m + G_m + B_f (\alpha + 1)) - \alpha J_m K_d) \quad (17)$$

$$d_6 = B_f J_m^2 \quad (18)$$

From Lemma 3, the non-negativeness of  $d_2$  imposes

$$K \geq \frac{\alpha}{\alpha + 1} K_d \quad (19)$$

Furthermore, the non-negativeness of  $d_6$  is guaranteed as the plant parameter  $B_f$  is positive. The last condition of Lemma 3 imposes

$$\begin{aligned} & -2 J_m \sqrt{B_f K (B_m + G_m) (K + \alpha (K - K_d))} \\ & \leq B_f ((B_m + G_m) (B_f (1 + \alpha) + B_m + G_m) - \alpha J_m K_d) \end{aligned} \quad (20)$$

which indicates  $(B_m + G_m) > 0$ .

3) Any poles of  $Z(s)$  on the imaginary axis are simple with positive and real residues. If  $B_m + G_m + B_f (\alpha + 1)$  and  $(\alpha + 1)$  are positive, then the only possible root on the imaginary axis is at zero with a residue of  $\frac{\alpha}{\alpha+1} K_d$ . Note that  $B_m + G_m + B_f (\alpha + 1) > 0$ , since Eqn. (20) implies that  $(B_m + G_m) > 0$ , and  $(\alpha + 1) > 0$  due to the stability condition. When  $(\alpha + 1) = 0$ , the output impedance transfer function becomes equal to  $\frac{B_f J_m s^3 + (B_f (B_m + G_m) + J_m K) s^2 + (K (B_m + G_m) - B_f K_d) s - K K_d}{J_m s^3 + (B_m + G_m) s^2}$  and Condition 3 of Theorem 1 is violated as double poles exist at  $s = 0$ . Hence, when  $(\alpha + 1) = 0$ , passive virtual springs cannot be rendered. ■

Passive Physical Equivalent: A realization of Eqn. (15) characterizing SDEA under VSIC during spring rendering when both controllers are proportional is presented in Figure 4h, where  $c_{1s} = \frac{K_d \alpha (B_f (B_m + G_m) - J_m K)}{B_f K (\alpha + 1)^2}$ ,  $b_{1s} = \frac{K_d \alpha (B_f (B_m + G_m) - J_m K)}{K^2 (\alpha + 1)^2}$ , and  $\sigma = \frac{1}{\alpha + 1} - \frac{\alpha}{(\alpha + 1)^2} \frac{K_d}{K}$ .

For the realization in Figure 4h to be feasible, all physical components of the model should be non-negative. Hence,  $(\alpha + 1)$  should be non-negative. Furthermore, the non-negativeness of the right spring imposes the condition expressed in Eqn. (19). The non-negativeness  $\sigma (B_m + G_m)$  is guaranteed if  $(B_m + G_m) \geq 0$  and Eqn. (19) are simultaneously satisfied. As  $\frac{\alpha}{\alpha+1} K_d$  approaches to zero, the outer spring which represents the virtual stiffness to be rendered, converges to zero. The conditions for the non-negativeness of  $c_{1s}$  and  $b_{1s}$  can be derived as

$$J_m \frac{K}{B_f} \leq (B_m + G_m) \quad (21)$$

which indicates  $(B_m + G_m) > 0$ .

Feasibility of Passive Realization vs Passivity: The feasibility conditions for the realization in Figure 4h provide sufficient conditions for the passivity of Eqn. (15). This can be shown by first considering a sufficient condition for the passivity that is ensured by imposing a non-negative value to  $d_4$  as follows

$$J_m \leq \frac{(B_m + G_m) (B_m + G_m + B_f (\alpha + 1))}{\alpha K_d} \quad (22)$$

Note that replacing the condition provided in Eqn. (20) with the non-negativeness of  $d_4$  provide a (more conservative) sufficient condition for the passivity. This condition still needs to be considered together with the other necessary conditions of non-negative  $d_2$  and  $d_6$ . Eqns. (21) and (22) can be arranged together as

$$J_m \leq \frac{(B_m + G_m) B_f}{K} \leq \frac{(B_m + G_m) (B_m + G_m + B_f (\alpha + 1))}{\alpha K_d} \quad (23)$$

Given Eqn. (19) as necessitated by the feasibility of the realization in Figure 4h and the passivity of Eqn. (15), this inequality is always satisfied. Therefore, Eqn. (21) is a more conservative sufficient condition than the one provided in Eqn. (22) and when Eqn. (21) is satisfied, Eqn. (20) is guaranteed to hold.

Hence, the realization in Figure 4h is feasible and the sufficient conditions for the passivity of Eqn. (15) are satisfied if the  $(B_m + G_m)$ ,  $(\alpha + 1)$ , and  $\frac{\alpha}{\alpha+1} K_d$  are positive, and Eqn. (21) is satisfied. If Eqn. (20) is replaced with Eqn. (21), then the necessary and sufficient conditions for the passivity of Eqn. (15) can be recovered.

## VI. HAPTIC RENDERING PERFORMANCE

In this section, we study the effects of the physical plant parameters and the controller gains on the rendering performance through Bode plots. We provide performance comparisons between different plants (e.g., SEA vs SDEA) and controller architectures (e.g., P-P vs P-PI), using the insight gained through the passive realizations of the closed-loop systems. We also evaluate the effective impedance of closed-loop systems through passive physical realizations.

The passive physical equivalents in Figure 4 explicitly show that, when causal controllers roll-off, the dynamics of the uncontrolled plant is recovered. Accordingly, the high frequency response of all realizations are dominated by the dynamics of the physical filters (spring and damper) serially attached to the plant; hence, passive physical realizations indicate that an SEA acts as a physical spring  $K$ , while an SDEA acts as a physical spring  $K$  and damping  $B_f$  in parallel, at high frequencies.

In Figure 4, all passive physical equivalents include an inerter and a damper term in parallel. This damper term significantly affects the low frequency range of null impedance and spring rendering, as well as the bandwidth of spring rendering. The inerter term affects the transition from the intermediate to the high frequency range.

Furthermore, in Figure 4, the passive physical equivalents for spring rendering include a spring  $\frac{\alpha}{\alpha+1} K_d$ , parallel to all other components. For large controller gains, this spring converges to the desired virtual spring  $K_d$  to be rendered. As the controllers are selected to include integral terms, additional

TABLE II: S(D)EA plant parameters used for the simulations

Parameter	$J_m$	$B_m$	$K$	$B_f$
Value	0.002 kg-m <sup>2</sup>	1.22 N-m s/rad	360 N-m/rad	0.5 N-m s/rad

components are included to the passive physical realizations, in parallel with the terms discussed above.

Table II presents the physical parameters of the S(D)EA plant used in simulations to evaluate the system performance. The proportional controller gains are set as  $G_m = 10$  N-m s/rad and  $G_t = 5$  rad/(s N-m), while the integral gain of the velocity controller is set as  $I_m = 10$  N-m/rad. Table I presents the numerical values selected for the parallel inerter and damping terms of the passive physical equivalents in Figures 4a–h for various controller gains  $G_m$ ,  $G_t$ ,  $I_m$ , and desired stiffness levels  $K_d$ .

Please note that only the parallel inerter and damper terms common to all realizations are presented in Table I. The parallel inerter and damper terms are equal to  $\frac{J_m}{\alpha+1}$  and  $\frac{B_m+G_m}{\alpha+1}$ , respectively, for all realizations in Figure 4 except three cases: the damper  $c_{1n}$  of SEA under VSIC during null impedance rendering when the motion controller is PI and the torque controller is P, the damper  $\sigma(B_m + G_m)$  and the inerter  $\sigma J_m$  of SEA under VSIC during spring rendering when the controllers are P, and the damper  $\sigma(B_m + G_m)$  of SDEA under VSIC during spring rendering when the controllers are P.

The null impedance rendering performance increases as the parallel inerter and damper terms in the physical equivalents decrease. From Table I, it can be observed that these parallel inerter and damper terms decrease with the choice of higher proportional gains  $G_t$  and  $G_m$ . For all physical equivalents,  $G_t$  has a larger effect on decreasing the damper term than  $G_m$ . Furthermore, the integral controller gain  $I_m$  does not have any significant effect on these parasitic inerter and damper terms, for the realizations considered, but results in a frequency dependent damping effect that increases with frequency.

The spring rendering performance also improves as the parasitic inerter and damper terms in the physical equivalents decrease. From Table I, it can be observed that these parallel inerter and damper terms decrease with the choice of higher proportional gains  $G_t$  and  $G_m$ . For all physical equivalents,  $G_t$  has a larger effect on decreasing the damper term than  $G_m$ .

TABLE I: Numerical values for the inerter and damping terms of the passive physical equivalents for SEA and SDEA for various controller gains  $G_m$ ,  $G_t$ ,  $I_m$ , and  $K_d$ . (Inerter is in kg-m<sup>2</sup> and damper is in N-m s/rad.)

	SEA				SDEA					
	Null Impedance Rendering				Spring Rendering		Null Impedance Rendering		Spring Rendering	
	P-P		P-PI		P-P		P-P		P-P	
	Inerter	Damper	Inerter	Damper ( $c_{1n}$ )	Inerter	Damper	Inerter	Damper	Inerter	Damper
$G_t = 5$	$3.92e^{-5}$	0.220	$3.92e^{-5}$	0.200	$2.32e^{-5}$	0.130	$3.92e^{-5}$	0.220	$3.92e^{-5}$	0.130
$G_t = 50$	$3.99e^{-6}$	0.022	$3.99e^{-6}$	0.020	$2.33e^{-6}$	0.013	$3.99e^{-6}$	0.022	$3.99e^{-6}$	0.013
$G_t = 100$	$2.00e^{-6}$	0.011	$2.00e^{-6}$	0.010	$1.17e^{-6}$	0.007	$2.00e^{-6}$	0.011	$2.00e^{-6}$	0.007
$G_m = 10$	$3.92e^{-5}$	0.220	$3.92e^{-5}$	0.200	$2.32e^{-5}$	0.130	$3.92e^{-5}$	0.220	$3.92e^{-5}$	0.130
$G_m = 50$	$7.97e^{-6}$	0.204	$7.97e^{-6}$	0.200	$4.66e^{-6}$	0.119	$7.97e^{-6}$	0.204	$7.97e^{-6}$	0.119
$G_m = 100$	$3.99e^{-6}$	0.202	$3.99e^{-6}$	0.200	$2.33e^{-6}$	0.118	$3.99e^{-6}$	0.202	$3.99e^{-6}$	0.118
$I_m = 10$	-	-	$3.92e^{-5}$	0.200	-	-	-	-	-	-
$I_m = 50$	-	-	$3.92e^{-5}$	0.200	-	-	-	-	-	-
$I_m = 100$	-	-	$3.92e^{-5}$	0.200	-	-	-	-	-	-
$K_d = 150$	-	-	-	-	$2.32e^{-5}$	0.130	-	-	$3.92e^{-5}$	0.130
$K_d = 200$	-	-	-	-	$1.79e^{-5}$	0.100	-	-	$3.92e^{-5}$	0.100
$K_d = 250$	-	-	-	-	$1.25e^{-5}$	0.070	-	-	$3.92e^{-5}$	0.070

Higher desired stiffness  $K_d$  decreases these parallel inerter and damper terms for SEA, while  $K_d$  decreases only the damper term and has no effect on the inerter term for SDEA.

Tables I show that the parasitic components of the physical realization approach to zero as the controller gains are increased; however, passivity bounds limit these gains to ensure that physical components do not become negative, resulting in a trade-off between the rendering performance and the stability robustness. Similarly, the passivity bounds impose an upper bound on  $K_d$  during spring rendering, as demonstrated by high  $K_d$  terms leading to negative damping in realizations.

#### A. Effects of Controller Gains on Null Impedance Rendering Performance

P-P controllers for SEA: Figure 4b indicates that the parasitic effect of the damper  $(B_m + G_m)/(\alpha + 1)$  and inerter  $J_m/(\alpha + 1)$  terms decrease with the choice of high controller gains for SEA during null impedance rendering when both controllers are P. It can be observed from Figure 4b that  $G_t$  has a more dominant effect on the damper term, while  $G_m$  and  $G_t$  gains affect the inerter term in the same manner, as their effects are multiplicative.

The effective impedance of the controllable part of the realization in Figure 4b, that is, the remaining system dynamics after the serial physical filter  $K$  is extracted, is dominated by the damper term  $(B_m + G_m)/(\alpha + 1)$  in the low frequency range. Therefore, the null impedance rendering performance can be increased in the low frequency range by attenuating the effects of this damper term. Similarly, the high frequency behaviour of these parasitic dynamics is dictated by the inerter  $J_m/(\alpha + 1)$  term. Hence, the passive physical equivalents provide an explicit representation for the effective impedance analysis.

Figure 5 presents Bode plots of system performance for various  $G_m$  and  $G_t$  controller gains. It can be observed from the Bode plots that the output impedance converges to the dynamics of the physical spring  $K$  at the high frequency range and the controller gains can shape this transition. Figure 5a indicates that the null impedance rendering performance can be significantly improved by employing higher  $G_t$  gains, leading to attenuated damping effects. Figure 5b shows that the effect of  $G_m$  gain is much less in the low frequency range.

Figures 5a and 5b indicate that higher  $G_t$  and  $G_m$  gains enable smoother the transition from the intermediate frequency range to the high frequency range and reduce the resonant peak. Table I can be used to verify that the damper term of passive physical equivalent decreases with choice of higher torque controller gain  $G_t$  and the inerter term decreases with choice of high controller gains  $G_t$  and  $G_m$ .

P-PI controllers for SEA: The Bode plots under P-PI controller are quite similar to the behaviour under the P-P control architecture as presented in Figure 5; hence, the effect of  $I_m$  on Bode plots of the null impedance rendering performance seems quite low. Bode plots of SEA under P-PI controllers are presented in the Supplementary Document [59].

Deeper insights may be gained by comparing the physical realization of these systems. In comparison to Figure 4b, Figure 4a indicates that the addition of an integral term to the motion controller modifies the damping term by splitting it into two parts: a regular damper  $c_{1n}$  whose damping coefficient is inversely proportional to  $G_t$  and a newly introduced element that consists of a damper  $c_{2n}$  in series with an inerter  $b_{1n}$ . The newly introduced serial damper-inerter term introduces frequency dependent dissipation to the system that increases with frequency.

These effects can be verified through an effective impedance analysis of the controllable part of the realization in Figure 4a. In particular, the effective damping for Eqn. (2) after removing the uncontrollable serial compliant element  $K$  can be computed as

$$c_{effP-PI}^{SEA}(\omega) = \frac{((B_m + G_m)(\alpha + 1) - G_t I_m J_m)\omega^2 + G_t I_m^2}{(\alpha + 1)^2 \omega^2 + G_t^2 I_m^2} \quad (24)$$

At low frequencies (as  $\omega \rightarrow 0$ ), Eqn. (24) converges to  $c_{1n}$ . At high frequencies (as  $\omega \rightarrow \infty$ ), Eqn. (24) approaches to  $c_{1n} + c_{2n}$ .

Similarly, the effective inertance for Eqn. (2) after removing the serial compliant element  $K$  can be computed as

$$b_{effP-PI}^{SEA}(\omega) = \frac{J_m(\alpha + 1)\omega^2 + I_m(B_m G_t - 1)}{(\alpha + 1)^2 \omega^2 + G_t^2 I_m^2} \quad (25)$$

At low frequencies (as  $\omega \rightarrow 0$ ), Eqn. (25) converges to  $\frac{J_m}{(\alpha + 1)} + b_{1n}$ . At high frequencies (as  $\omega \rightarrow \infty$ ), Eqn. (25) approaches to  $\frac{J_m}{\alpha + 1}$ .

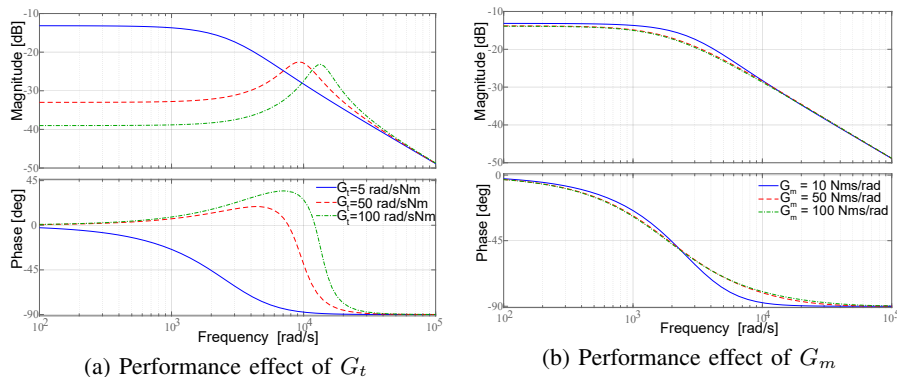


Fig. 5: Effect of  $G_t$  and  $G_m$  on null impedance rendering performance of SEA when both controllers are P

Hence, the null impedance rendering performance at the low frequency range is dominated by the parasitic damping of  $c_{1n}$ , while a parasitic inertia of  $\frac{J_m}{(\alpha+1)} + b_{1n}$  acts at this frequency range. The parasitic damping term  $c_{1n}$  is inversely proportional to  $G_t$  and can be attenuated by the torque controller. Similarly, the parasitic inertia  $\frac{B_m G_t - 1}{G_t I_m}$  at the low frequency range can be attenuated by  $G_t$  and  $I_m$  gains. As can be observed from the physical realization,  $I_m$  and  $G_m$  do not affect  $c_{1n}$ . Furthermore,  $G_m$  does not affect parasitic inertia at the low frequency range. At intermediate frequencies,  $c_{2n}$  slightly reduces with higher  $I_m$  selections, so the performance of null impedance rendering can be mildly improved by  $I_m$ .

While  $I_m$  does not display a noticeable effect on the null impedance rendering performance,  $I_m$  significantly affects the disturbance rejection performance of the system, as the disturbance rejection performance is improved by larger  $I_m$  gains. Further insight into the disturbance rejection performance can also be gained through physical realizations. In particular, if we consider a disturbance torque  $F_{dist}$  acting on the system at the same location with the actuator input in Figure 1, the disturbance response of the closed-loop system under P-PI VSIC controller during null impedance rendering can be derived as

$$Y_{f_{null}}^{SEA^{P-PI}}(s) = \frac{\omega_{end}}{F_{dist}} \Big|_{\tau_{sea}=0} = \frac{s}{J_m s^2 + (B_m + G_m) s + I_m} \quad (26)$$

The disturbance transfer function  $Y_{f_{null}}^{SEA^{P-PI}}$  in Eqn. (26) is in the form of a passive admittance of an inerter  $J_m$ , damper  $(B_m + G_m)$  and spring  $I_m$  in parallel; hence,  $Y_{f_{null}}^{SEA^{P-PI}}$  decreases with  $I_m$ , indicating better disturbance attenuation. The physical realization of  $Y_{f_{null}}^{SEA^{P-PI}}$  emphasizes the effect of  $I_m$  as the restoring spring that counteracts disturbances.

When a P-P controller that omits the integral term is utilized under VSIC, no restoring spring exists for the disturbance response and larger steady state errors are likely be induced due to disturbances. Also note that larger  $G_m$  gains positively impact the disturbance response of both systems.

**P-P controllers for SDEA:** The physical realization of SDEA during null impedance rendering is identical to that of SEA, except the fact that the physical filter of SDEA includes a physical damping term  $B_f$  parallel to the physical spring  $K$ .

Similar to the case with SEA, Figure 4f indicates that the parasitic effect of the damper  $(B_m + G_m)/(\alpha + 1)$  and the inerter  $J_m/(\alpha + 1)$  terms decrease with the choice of high controller gains for SDEA during null impedance rendering when both controllers are P.  $G_t$  has a more dominant effect on the damper term, while  $G_m$  and  $G_t$  gains affect the inerter term in the same manner, as their effects are multiplicative.

The effective impedance of the controllable part of the realization in Figure 4f, that is, the remaining system dynamics after the serial physical filter consisting of  $K$ - $B_f$  terms is extracted, is dominated by the damper term  $(B_m + G_m)/(\alpha + 1)$  in the low frequency range. Therefore, the null impedance rendering performance can be increased in the low frequency range by attenuating the affects of this damper term. Similarly, the high frequency behaviour of the parasitic dynamics is dictated by the inerter  $J_m/(\alpha + 1)$  term. Bode plots of SDEA during null impedance rendering when both controllers are P are presented in the Supplementary Document [59].

### B. Effects of Controller Gains on Ideal Spring Rendering Performance

**P-P Controllers for SEA:** The physical realization of SEA during ideal spring rendering in Figure 4d indicates two branches in parallel: an ideal spring  $\frac{\alpha K_d}{(\alpha+1)}$  whose stiffness approaches to the desired spring  $K_d$  as the controller gains gets large and parasitic dynamics governed by a damper-inertance pair in parallel that is coupled to the system with a spring in series. The stiffness of the coupling spring is given by  $K - \frac{\alpha K_d}{(\alpha+1)}$ ; hence, the parasitic dynamics gets more decoupled from the system as the as the controller gains  $G_t$  and  $G_m$  increase. Note that, since the coupling spring needs to be positive for feasibility, this springs imposes an upper bound on  $K_d$  that can be passively rendered. The parasitic damper-inertance dynamics is scaled by  $\sigma = \frac{1}{\alpha+1} - \frac{\alpha}{(\alpha+1)^2} \frac{K_d}{K}$ , indicating that  $G_t$  has a significant effect for damper term, while both  $G_m$  and  $G_t$  equally affect the inerter term. Furthermore, the parasitic dynamics decrease with the choice of higher  $K_d$  values. When  $K_d = 0$ , the parasitic dynamics converges to that of null impedance rendering.

Since high frequency dynamics of SEA is governed by the spring of the physical filter, all Bode plots converge to

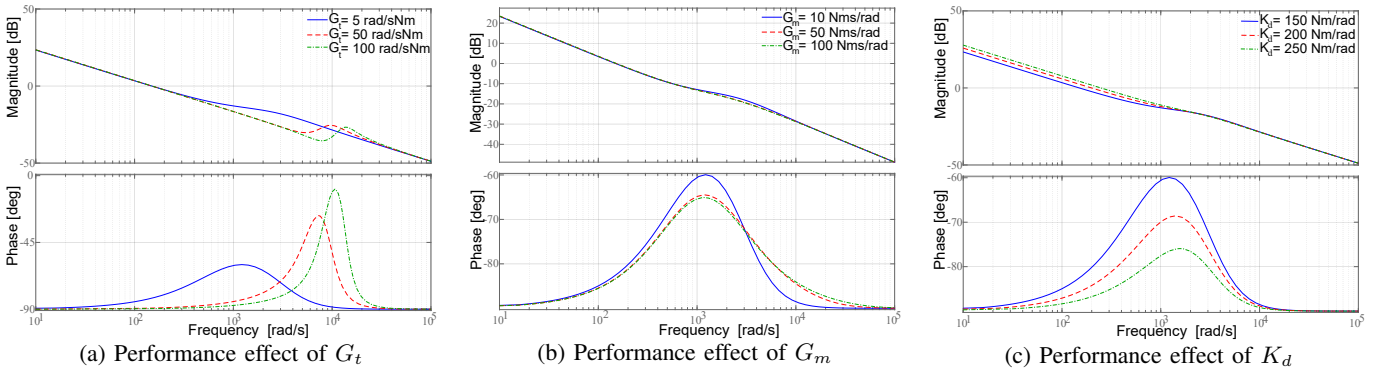


Fig. 6: Effect of  $G_t$ ,  $G_m$ , and  $K_d$  on the spring rendering performance of SEA during when both controllers are P

this dynamics. Figure 6a shows that as the torque controller gain  $G_t$  is increased, the frequency range over which the virtual stiffness is successfully rendered can be significantly increased. Figures 6a and 6b indicate that, a smoother transition takes place at the intermediate frequency range, from the rendered virtual spring at the low frequency range to the spring of the physical filter at the high frequency range, when higher P-gains are utilized. Similarly, Figure 6c shows that higher virtual stiffness levels can be rendered for higher  $K_d$  selections, and for such selections the transition at the intermediate frequency range is smoother. Figure 6b indicates that  $G_m$  gains do not result in significant rendering performance differences at the low frequency range; however,  $G_m$  gains positively impact the disturbance response of the system, as shown in the previous subsection. Furthermore, the effects of controller gains on parameters of the realization can also be verified through the numerical values presented in Table I.

Insight into the disturbance rejection performance of SEA during spring rendering can also be gained through physical realizations. In particular, if we consider a disturbance torque  $F_{dist}$  acting on the system at the same location with the actuator input in Figure 1, the disturbance response of the closed-loop SEA system under P-P VSIC controller during spring rendering can be derived as

$$Y_{f_{spring}}^{SEA^{P-P}}(s) = \frac{\omega_{end}}{F_{dist}} \Big|_{\tau_{sea}=0} = \frac{s}{J_m s^2 + (B_m + G_m)s + G_m G_t K_d} \quad (27)$$

The disturbance transfer function  $Y_{f_{spring}}^{SEA^{P-P}}$  in Eqn. (27) is in the form of a passive admittance of an inerter  $J_m$ , damper  $(B_m + G_m)$  and spring  $G_m G_t K_d$  in parallel; hence,  $Y_{f_{spring}}^{SEA^{P-P}}$  decreases with larger controller gains and  $K_d$ , indicating better disturbance attenuation. The physical realization of  $Y_{f_{spring}}^{SEA^{P-P}}$  emphasizes the effect of  $G_m G_t K_d$  as the restoring spring that counteracts disturbances. Note that when  $K_d \rightarrow 0$ , the disturbance response for null impedance rendering case is recovered.

**P-P Controllers for SDEA:** The physical realization of SDEA during ideal spring rendering is related to that of SEA in a number of ways. Similar to the case for SEA, Figure 4h indicates two branches in parallel: an ideal spring  $\frac{\alpha K_d}{(\alpha+1)}$  whose stiffness approaches to the desired spring  $K_d$  as the controller gains gets large and parasitic dynamics governed by damper-inertance elements that are serially coupled to the system with a spring-damper pair in parallel. The main differences are due to the physical filter damping  $B_f$  appearing in parallel to the coupling spring  $K - \frac{\alpha K_d}{(\alpha+1)}$  and the more complicated form of the parasitic damper-inertance dynamics.

Existence of the physical filter damping  $B_f$  in parallel to the coupling spring indicates that, unlike the case in SEA, the parasitic dynamics cannot be completely decoupled from the system as the controller gains  $G_t$  and  $G_m$  increase, since  $B_f$  term dominates the coupling at the intermediate and high frequencies. Similar to the case with SEA, Figure 4h indicates that the parasitic effects of the damper  $\sigma(B_m + G_m)$  and the inerter  $J_m/(\alpha + 1)$  terms decrease with the choice of high

controller gains. Once again,  $G_t$  has a more dominant effect on the damper term, while  $G_m$  and  $G_t$  gains affect the inerter term in the same manner, as they are multiplicative. Note that the topology of the parasitic damper-inertance dynamics are similar to that of the parasitic dynamics when SEA is under PI motion controller as shown in Figure 4c, whose components are presented in the Supplementary Document [59]. In comparison to Figure 4d, Figure 4h indicates that the addition of a physical damping  $B_f$  to the filter appends the parasitic dissipation effects by introducing a serial damper-inerter term that introduces frequency dependent dissipation to the system whose effect increases with frequency.

These effects can be verified through an effective impedance analysis of the parasitic dynamics of the realization in Figure 4h. In particular, the effective damping for Eqn. (15) after removing the serial coupling filter  $B_f - \left(K - \frac{\alpha K_d}{(\alpha+1)}\right)$  pair and the rendered stiffness  $\frac{\alpha K_d}{(\alpha+1)}$  can be computed as

$$c_{effPP}^{SDEA} = \frac{B_f (B_f (B_m + G_m)(\alpha + 1) - J_m K_d \alpha) \omega^2 + K (K (B_m + G_m)(\alpha + 1) - K_d \alpha (B_m + G_m))}{B_f^2 (\alpha + 1)^2 \omega^2 + K^2 (\alpha + 1)^2} \quad (28)$$

At low frequencies (as  $\omega \rightarrow 0$ ), Eqn. (28) converges to  $\sigma(B_m + G_m)$ . At high frequencies (as  $\omega \rightarrow \infty$ ), Eqn. (28) approaches to  $\sigma(B_m + G_m) + c_{1s}$ .

Similarly, the effective inertance for the parasitic dynamics of Eqn. (15) can be computed as

$$b_{effPP}^{SDEA} = \frac{(B_f^2 J_m (\alpha + 1)) \omega^2 + J_m K^2 (\alpha + 1) + B_f K_d \alpha (B_m + G_m) - J_m K K_d \alpha}{B_f^2 (\alpha + 1)^2 \omega^2 + K^2 (\alpha + 1)^2} \quad (29)$$

At low frequencies (as  $\omega \rightarrow 0$ ), Eqn. (29) converges to  $\frac{J_m}{\alpha+1} + b_{1s}$ . At high frequencies (as  $\omega \rightarrow \infty$ ), Eqn. (29) approaches to  $\frac{J_m}{\alpha+1}$ .

Similar to the case with SEA, the ideal spring impedance rendering performance at the low frequency range is dominated by the parasitic damping of  $\sigma(B_m + G_m)$ , while a parasitic inertance of  $\frac{J_m}{(\alpha+1)} + b_{1s}$  acts at this frequency range. Hence, the parasitic damping at low frequencies can be effectively attenuated by the torque controller  $G_t$ . Similarly, the parasitic inertance  $\frac{J_m}{(\alpha+1)}$  at the high frequency range can be attenuated by  $G_t$  and  $G_m$  gains.

Since the high frequency dynamics of SDEA is governed by the damping of the physical filter, all Bode plots converges to this dynamics. Along these lines, the high frequency behaviour of SDEA is significantly different from that of SEA.

If we consider a disturbance torque  $F_{dist}$  acting on the system at the same location with the actuator input in Figure 1, the disturbance response  $Y_{f_{spring}}^{SDEA^{P-P}}(s)$  of the closed-loop SDEA system under P-P VSIC controller during spring rendering is identical to that of SEA given in Eqn. (27). Hence, the addition of  $B_f$  to the physical filter does not affect this disturbance response.

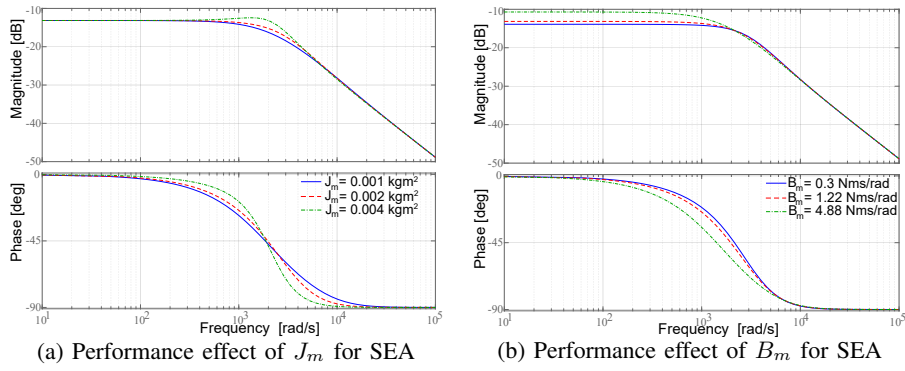


Fig. 7: Effect of plant parameters  $J_m$  and  $B_m$  on performance of SEA and SDEA during null impedance rendering when both controllers are P

### C. Effects of Physical Plant and Filter Parameters on Null Impedance Rendering Performance

Passive physical equivalents do not distinguish between the plant parameters and the controller gains and promote co-design thinking by enforcing simultaneous and unbiased consideration of controller and plant dynamics on the closed-loop system performance [60], [61].

Effects of Plant Parameters: Figures 4b and 4f indicate that the inerter term is equal to  $\frac{J_m}{\alpha+1}$  for S(D)EA during null impedance rendering when both controllers are P. Hence, the parasitic effect of this intertence can be reduced, either by redesigning the plant with a lower  $J_m$  or selecting higher controller gains. Figure 7a shows that better null impedance rendering performance can be achieved by employing a lower  $J_m$  for SEA plants.

Similarly, Figures 4b and 4f indicate that the damper term is equal to  $\frac{B_m + G_m}{\alpha+1}$  for S(D)EA during null impedance rendering when both controllers are P. Hence, the parasitic effect of this damper can be reduced, either by redesigning the plant with a lower  $B_m$  or selecting higher controller gains, especially higher  $G_t$ . Figure 7b shows that the null impedance rendering performance can be improved by employing a lower  $B_m$  for SEA plants. Bode plots of SDEA for various  $J_m$  and  $B_m$  are presented in the Supplementary Document [59].

Effects of Physical Filter Parameters: Figures 4b and 4f indicate that the physical filter affects the system performance

as a serially connected mechanical low-pass filter and does not have any influence on the remaining parasitic dynamics. Figures 8a and 8b indicate that the null impedance rendering bandwidth of S(D)EA improves for the selection of higher filter stiffness  $K$ , when both controllers are P.

This performance improvement is due to the improved bandwidth of the physical filter; however, employing a stiffer mechanical filter comes with the cost of reduced force sensing resolution and less disturbance attenuation under impulsive disturbances acting at the interaction port.

Figure 8c shows that the damping of the physical filter  $B_f$  dominate the high frequency dynamic behaviour of SDEA.

### D. Effects of Physical Plant and Filter Parameters on Ideal Spring Rendering Performance

Effects of Plant Parameters: Figures 4d and 4h indicate that the inerter terms are equal to  $\sigma J_m$  and  $\frac{J_m}{\alpha+1}$  for SEA and SDEA, respectively, during ideal spring rendering when both controllers are P. Hence, the parasitic effect of these intertences can be reduced, either by redesigning the plant with a lower  $J_m$  or selecting higher controller gains. Figure 9a shows that better virtual spring rendering performance can be achieved by employing a lower  $J_m$  for SEA plants.

Similarly, Figures 4d and 4h indicate that the low frequency dominant damper term is equal to  $\sigma(B_m + G_m)$  for both SEA and SDEA during ideal spring rendering when both controllers are P. Hence, the parasitic effect of this damper

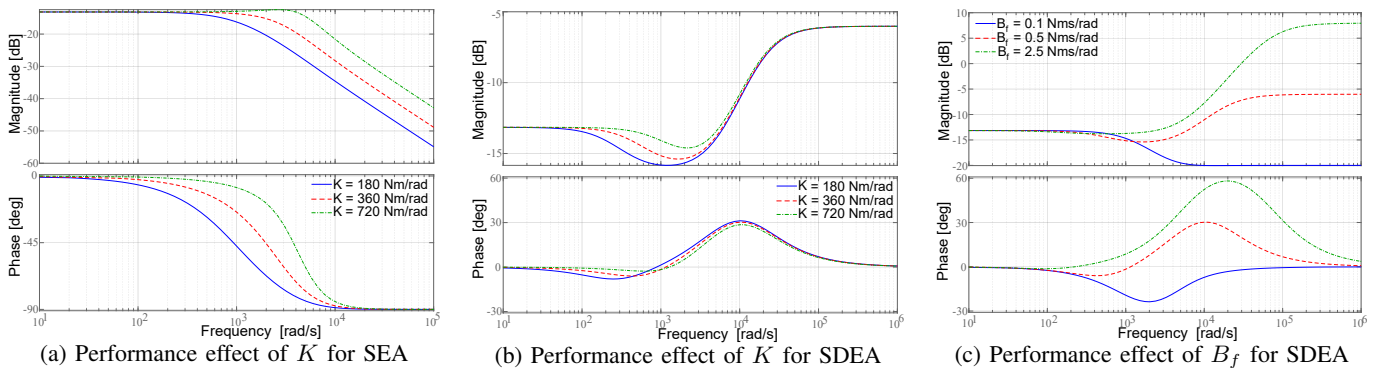


Fig. 8: Effect of physical filter parameters  $K$ - $B_f$  on performance of SEA and SDEA during null impedance rendering when both controllers are P

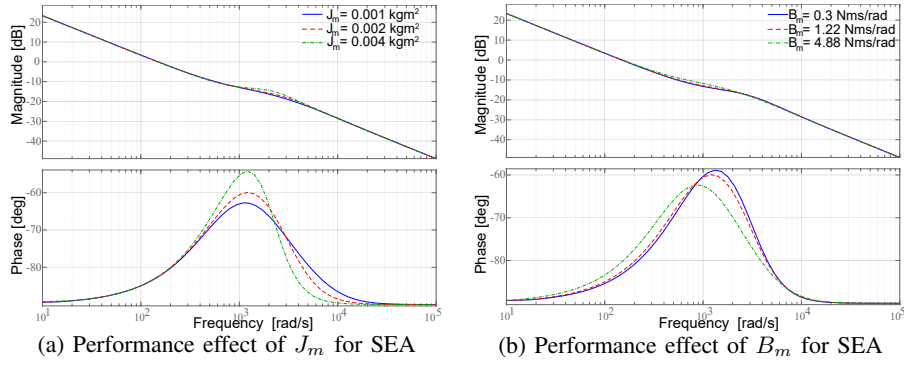


Fig. 9: Effect of plant parameters  $J_m$  and  $B_m$  on performance of SEA and SDEA during ideal spring rendering when both controllers are P

can be reduced, either by redesigning the plant with a lower  $B_m$  or selecting higher controller gains, especially higher  $G_t$ . Figure 9b shows that the virtual spring rendering performance can be improved by employing a lower  $B_m$  for SEA plants. Bode plots of SDEA for various  $J_m$  and  $B_m$  are presented in the Supplementary Document [59].

**Effects of Physical Filter Parameters:** Figures 4d and 4h indicate that the physical filter directly affects the virtual spring rendering performance of the system, as it acts as the coupling element between the parasitic system dynamics and spring to be rendered. In particular, the coupling spring is in the form of  $K - \frac{\alpha K_d}{\alpha+1}$ , whose feasibility of implementation imposes an upper bound on the virtual springs  $K_d$  that can be passively rendered. The effect of coupling through this spring element can be reduced by using a physical filter with lower stiffness  $K$ .

Furthermore, the stiffness of the physical filter  $K$  has a direct effect on the term  $\sigma$  that scales parasitic dynamic effects. In particular,  $\sigma = \frac{1}{\alpha+1} - \frac{\alpha}{(\alpha+1)^2} \frac{K_d}{K}$  can be reduced by the use of lower filter stiffness  $K$ , positively affecting the parasitic inertia and damping effects for SEA, and damping effects for SDEA, respectively.

Figure 4h indicates that the damper of the physical filter  $B_f$  directly affects the coupling behaviour and lower  $B_f$  increases the range of virtual stiffness, while the accuracy of virtual stiffness decreases.

Figures 10a and 10b show that the frequency range over

which desired virtual spring is rendered can be improved if the stiffness of the physical filter  $K$  is selected to be close to  $K_d$ . Figure 10c indicates that the range of the virtual spring rendering is improved with less accuracy for lower  $B_f$ , as this damping dominates the high frequency behaviour and the transition from the desired spring to  $B_f$  needs to take place earlier for larger  $B_f$ .

#### E. Rendering Performance Comparison of SEA vs SDEA

For null impedance rendering, Figures 4b and 4f indicate that both SEA and SDEA have identical parasitic dynamics consisting of a damper and inerter in parallel and the effects of controller gains on these elements are the same. Hence, only difference is due to the damper term  $B_f$  in the physical filter of SDEA. Figure 11a presents a comparison the null impedance rendering performance of SEA and SDEA when the controller gains are selected to be the same. As can be verified from Table I, the inerter and damper terms of physical equivalents of SEA and SDEA have the same values. Figure 11a indicates that the performance of SEA and SDEA are very close in the low frequency range. However, as expected, the high frequency dynamics of SEA is dominated by the stiffness of the physical filter, while the high frequency dynamics of SDEA is dominated by the damping of the physical filter. Hence, the transition from null impedance rendering to high frequency dynamics differs significantly for SEA and SDEA.

For ideal spring rendering, Figures 4d and 4h indicate

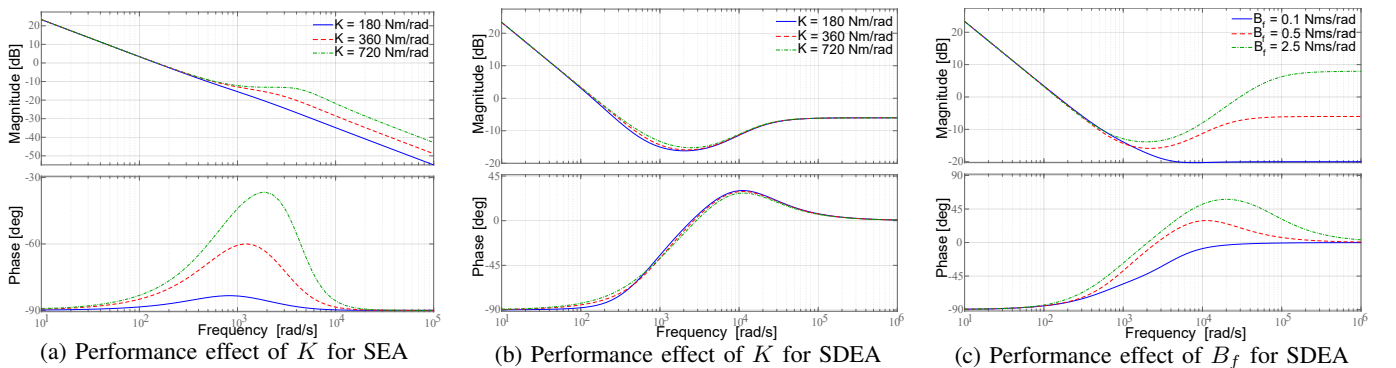


Fig. 10: Effect of physical filter parameters  $K$ - $B_f$  on performance of SEA and SDEA during ideal spring rendering when both controllers are P

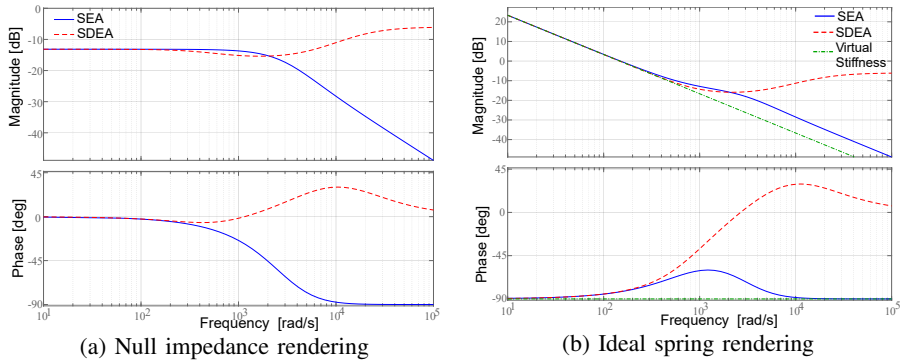


Fig. 11: Rendering performance comparison between SEA and SDEA

that both SEA and SDEA include identical parasitic damper terms, but the parasitic inerter terms are different. Furthermore, SDEA includes an extra branch with frequency dependent damping effect that increases with frequency. As can be verified from Table I, the inerter effects are lower for SEA, compared to SDEA, while the low frequency damping effects are identical. Figure 11b presents a comparison the ideal spring impedance rendering performance of SEA and SDEA when the controller gains are selected to be the same.

Similar to the the null impedance rendering case, the high frequency dynamics of SEA is dominated by the stiffness  $K$  of the physical filter, while the high frequency dynamics of SDEA is dominated by the damping  $B_f$  of the physical filter. Accordingly, the transition from spring rendering to high frequency dynamics differs significantly for SEA and SDEA.

## VII. EXPERIMENTAL VALIDATION

In this section, we experimentally validate the theoretical passivity bounds and the haptic rendering performance of S(D)EA using a customized version of the single degree of freedom series elastic brake pedal presented in [62], [63]. The series elastic brake pedal, presented in Figure 12, is actuated by a brushless DC motor equipped with a Hall-effect sensor and an optical encoder. The torque output of the motor is amplified with a gearbox and a capstan reduction featuring 1:10 and 1:3.95 transmission ratios, respectively. The series elastic element is implemented as an ideal spring through a compliant cross-flexure joint embedded into the capstan pulley. The deflections of the cross-flexure joint are measured through a linear encoder to estimate the interaction torques. All controllers are implemented in real-time at 1 kHz utilizing an industrial PC connected to an EtherCAT bus.

To implement a series *damped* elastic brake pedal, linear eddy current damping is added in parallel to the compliant element of the SEA brake pedal. In particular, permanent magnets arranged as a Halbach array to augment the magnetic field on the side of the array are placed to face an aluminum plate. The distance between the magnet array and aluminum plate is adjusted to control the level of viscous damping added to the system. When the magnets are removed, the SDEA brake pedal simplifies to the SEA brake pedal.

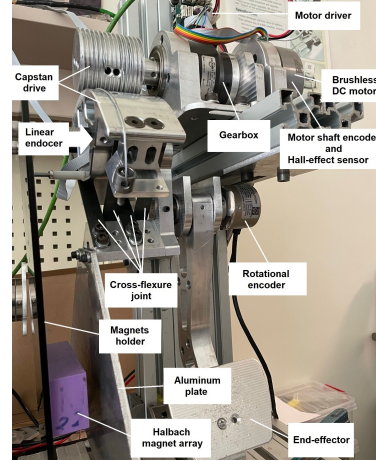


Fig. 12: Experimental setup: The S(D)EA brake pedal

### A. Identification of Plant Parameters

Accurate determination of the plant parameters is important to verify the passivity bounds of the system. First, the stiffness and damping of the physical filter are identified, respectively.

The stiffness of the cross-flexure joint is experimentally determined by applying pre-determined torques to the end-effector and measuring the resulting deflections when the actuator is locked. A least square fit to the experimental data indicates that  $K = 121.8$  N-m/rad with  $R^2 = 0.99$ .

For the system identification of the damping coefficient, the magnet array is fixed to a force sensor and the motion of the aluminum plate is controlled to follow a reference chirp signal with an amplitude of 33.5 rad/sec over the frequency range of 0.9-1.4 Hz. The velocity is estimated through the numerical differentiation of the encoder data using the curve braking velocity estimator [64]. A least square fit to the experimental data indicates that  $B_f = 0.0127$  N-m s/rad with  $R^2 = 0.84$ .

Closed-loop system identification is utilized to experimentally determine the system parameters related to the actuator and the power transmission. The closed-loop identification enables accurate prediction of the plant parameters using LTI techniques, since the robust motion controller effectively compensates for the hard-to-model nonlinear effects in the power transmission. To determine the reflected inertia and damping of the plant, the system identification is performed under the inner velocity controller with  $G_m = 0.0576$  N-

m/s/rad. A chirp velocity reference signal with an amplitude of 7.85 rad/sec is applied to the motion control loop over the frequency range of 0.001-10 Hz, while no exogenous torque  $\tau_{sea}$  is applied to the system. A first-order transfer function is fitted to the collected data to determine the plant parameters as  $J_m = 0.0024 \text{ kg}\cdot\text{m}^2$  and  $B_m = 0.0177 \text{ N}\cdot\text{m s/rad}$  with  $R^2 = 0.88$ . Unless otherwise stated, the controller gains of VSIC are set to  $G_m = 0.0576 \text{ N}\cdot\text{m/s/rad}$  and  $G_t = 25 \text{ rad/(s}\cdot\text{N}\cdot\text{m)}$ .

### B. Verification of Passivity Bounds

The challenging nature of the experimental determination of closed-loop system phase with high accuracy and repeatability renders the empirical verification of system passivity through Bode plots unreliable. On the other hand, it has been established in the literature that the passivity of a system can also be investigated by studying the coupled stability of interactions when the system is exposed to most destabilizing environments [65]. In particular, passivity can be concluded if and only if there exists no set of ideal springs or inertias that destabilize the system under excitations that span the whole frequency spectrum [21]. For SEA, inertial environments have been determined to be the most destabilizing [66].

To validate the theoretical passivity bounds established in this paper, the S(D)EA brake pedal is coupled to a range of inertias and impacts are imposed to the end-effector to excite the system at all possible frequencies. If the violation of coupled stability (e.g., chatter) is observed, then the system is not passive. If no violation of the coupled stability is observed after many trials during which the end-effector inertia of the S(D)EA brake pedal is gradually increased, then it is concluded that the experimental evidence indicates the passivity of the system.

Please note that, for simplicity of presentation, the theoretical passivity bounds in the previous sections have been derived under the non-limiting assumption that the power transmission of the system has a unity reduction ratio. Equivalent plant parameters and controller gains can be established for systems with a reduction ratio of  $n$  by introducing the following mappings:  $J_{meq} = n^2 J_m$ ,  $B_{meq} = n^2 B_m$ , and  $G_{meq} = n^2 G_m$ , and  $G_{teq} = 1/n G_t$ .

### Null Impedance Rendering with SEA

In these experiments, we have studied the coupled stability of SEA under VSIC during null impedance rendering when the controllers are P-PI. We have selected one passive and one active  $G_t$  gains for five distinct  $I_m$  gains according to the necessary and sufficient condition given in Eqn. (6).

Figure 13a presents the experimental  $G_t$ - $I_m$  plot for the SEA brake pedal, together with the theoretically predicted passivity boundary depicted as the magenta line. The symbols “\*” indicate the experiments where coupled stability was preserved, while symbols “o” denote the experiments where coupled stability was compromised. As can be inspected from Figure 13a, the test cases are fairly close to the analytically predicted passivity boundary and these results serve as a validation of the theoretical passivity bound. These results also indicate that the modelling assumptions considered during the theoretical derivations are reasonable and do not cause large deviations from the theoretical predictions.

### Spring Rendering with SEA

In these experiments, we have studied the coupled stability of SEA under VSIC during spring rendering when both controllers are P. We have selected one passive and one active  $K_d$  values for four distinct  $G_t$  gains according to the necessary and sufficient condition given in Eqn. (10).

Figure 13b presents the experimental  $K_{vir}$ - $G_t$  plot for the SEA brake pedal, where  $K_{vir} = \frac{\alpha}{\alpha+1} K_d$  denotes the stiffness of rendered spring. In the figure, the theoretical passivity boundary is depicted as the magenta line and equal to physical stiffness of the SEA according to Eqn. (10). The experimental results validate the analytically predicted passivity boundary. According to the experimental results, the theoretical bound is about 7% more conservative, as the physical system is likely to have some extra dissipation due to unmodelled friction and hysteresis effects.

### Spring Rendering with SDEA

In these experiments, we have studied the coupled stability of SDEA under VSIC during spring rendering when both controllers are P. We have selected one passive and one active  $K_d$  values for four distinct  $G_t$  gains according to the necessary

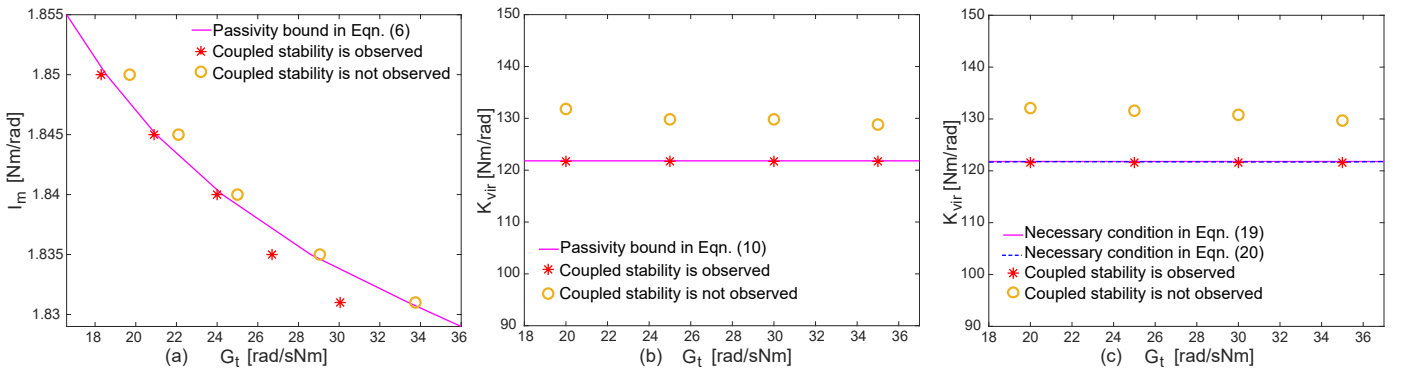


Fig. 13: Passivity bounds vs experimentally determined coupled stability: (a)  $I_m$ - $G_t$  plot for SEA during null impedance rendering, (b)  $G_t$ - $K_{vir}$  plot for SEA during spring rendering, and (c)  $G_t$ - $K_{vir}$  plot for SDEA during spring rendering.

and sufficient conditions given in Eqns. (19) and (20).

Figure 13c presents the experimental  $K_{vir}-G_t$  plot for the SDEA brake pedal. In the figure, the theoretical passivity bound according to Eqn. (19) is depicted as the magenta line and equal to physical stiffness of the SDEA, while the bound according to Eqn. (20) is depicted as the blue line. Figure 13c shows that the two conditions are very close to each other for the parameters of the SDEA brake pedal. The experimental results validate the analytically predicted passivity boundary. According to the experimental results, the theoretical bounds are about 6.5% more conservative, as the physical system is likely to have some extra dissipation due to unmodelled friction and hysteresis effects.

### C. Evaluation of Haptic Rendering Fidelity

In this subsection, we have experimentally evaluated the performance of S(D)EA under VSIC during null impedance and spring rendering. Since the haptic rendering performance of SDEA under VSIC is very similar to that of SEA for the S(D)EA brake pedal, only the results for SEA are provided for the brevity of the presentation.

#### Null Impedance Rendering with SEA

The performance of SEA under VSIC during null impedance rendering is important, as this control mode provides active backdrivability to the system to allow users to move the system without much resistance.

Figure 14a presents the null impedance rendering performance of SEA under VSIC for three distinct levels of the torque controller gain  $G_t$ . As the torque controller gain  $G_t$  is increased from 20 rad/(s N-m) to 30 rad/(s N-m), the torque required to move the pedal decreases from 1.48% to 0.62% of 40 N-m torque output capacity of the SEA brake pedal. Note that this level of active-backdrivability is excellent for the SEA brake pedal, as evidenced by commonly employed chip test, where a potato chip is used to move the device without getting broken. The experimental results in Figure 14a are also in good agreement with the analysis presented in Section VI, where the positive effect of increasing the torque controller gain  $G_t$  on the null impedance rendering performance has been shown.

#### Spring Rendering with SEA

The performance of SEA under VSIC during spring rendering is important, as this control mode is commonly used to implement virtual constraints to avoid users to reach the undesired regions of the workspace.

Figure 14b presents the experimental verification of the spring rendering performance for two distinct levels of virtual stiffness, where  $K_d = 50$  and 100 N-m/rad when  $G_t = 30$  rad/(s N-m). The rendered stiffness of the SEA under VSIC is experimentally determined by applying pre-determined torques to the end-effector and measuring the resulting deflections. A least square fit to the experimental data indicates that  $K_{vir} = 51.11$  N-m/rad with  $R^2 = 0.99$  and  $K_{vir} = 98.36$  N-m/rad with  $R^2 = 0.99$ , resulting in 3.73% error for  $K_d = 50$  N-m/rad and 0.19% error for  $K_d = 100$  N-m/rad, respectively. These experiments are repeated for  $G_t = 25$  rad/(s N-m). In this case, a least square fit to the experimental data indicates that  $K_{vir} = 51.27$  N-m/rad with  $R^2 = 0.99$  and  $K_{vir} = 98.99$  N-m/rad with  $R^2 = 0.99$ , resulting in 4.35% error for  $K_d = 50$  N-m/rad and 0.73% error for  $K_d = 100$  N-m/rad, respectively. The experimental results in Figure 14b are in good agreement with the analysis presented in Section VI, where the positive effects of increasing the torque controller gain  $G_t$  and desired virtual stiffness  $K_d$  on the spring rendering performance have been shown.

Figure 14c presents the interaction performance of the SEA brake pedal under dynamic inputs from a user. During these experiment, the SEA brake pedal was rendering a virtual stiffness of  $K_d = 50$  N-m/rad with  $G_t = 30$  rad/(s N-m). The desired interaction torque due to the virtual stiffness model and the interaction torques estimated through the series elastic elements are presented with dashed and solid lines, respectively. The normalized RMS error for this dynamic tracking task is computed as 3.03%. This experiment was also repeated for  $G_t = 25$  rad/(s N-m). In this case, the normalized RMS error is computed as 3.28%. These experimental results are in good agreement with the analysis presented in Section VI, where it has been demonstrated that increasing the torque controller gain  $G_t$  improves the force tracking performance.

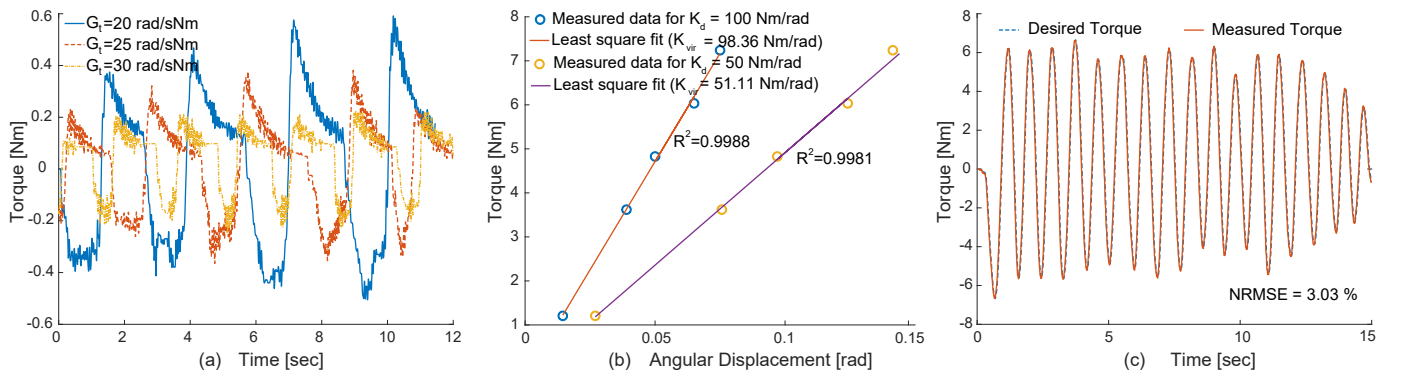


Fig. 14: (a) Null impedance rendering performance (potato chip) test for  $G_t = 20, 25$  and  $30$  rad/(s N-m), (b) Virtual stiffness rendering for  $K_d = 50$  and  $100$  N-m/rad when  $G_t = 30$  rad/(s N-m), and (c) Tracking performance of SEA during virtual spring rendering with  $K_d = 100$  N-m/rad and  $G_t = 30$  rad/(s N-m).

## VIII. CONCLUSIONS AND DISCUSSION

In Sections IV and V, we have presented the frequency domain passivity analysis of SEA and SDEA under VSIC for null impedance rendering and spring rendering, and provided the necessary and sufficient conditions for the passivity of these systems. These results extend earlier results on S(D)EA passivity in the literature [21], [25], [26], as the controller gains are allowed to take negative values. In addition to the passivity analysis, we have derived passive physical equivalents for these systems which provide novel insights and intuition into the closed-loop system dynamics. In particular, the passive physical equivalents make the parasitic dynamics of the system explicit and enable rigorous study of system parameters and controller gains on the rendering performance.

The passive physical equivalents not only provide a concrete understanding of uncontrollable dynamics of the closed-loop system (e.g., the dynamics of the physical filter is uncontrollable during null impedance rendering under VSIC), but also enable an understanding of the limitations of rendering performance (e.g., the stiffness of the physical stiffness provides an upper bound on virtual spring rendering under VSIC). Note that these results extend the interaction stability analysis in [27] to S(D)EA and provide easy-to-understand insights into the fundamental limitations and robust stability-transparency trade-off of S(D)EA.

In Section VI, we have demonstrated that passive physical equivalents enable fair comparisons of different plants (e.g., SEA vs SDEA) and different controllers (e.g., P-P vs P-PI) on the haptic rendering performance. Unlike the case in numerical studies, comparisons of closed-loop system dynamics through passive physical equivalents are informative in that these conclusions can be generalized. These comparisons highlight the impact of different plant and controller terms on the closed-loop rendering performance. Furthermore, there exists continuity among realizations; for instance, one can recover the realization of null impedance rendering with SEA under P-P controller from the realization of spring rendering with SDEA under P-PI controller, by setting  $B_f$ ,  $I_m$ , and  $K_d$  to zero. Along these lines, the effect of each additional controller terms or plant dynamics can be rigorously studied.

Moreover, these comparisons are symbolic in nature and do not require performance optimization of each closed-loop system to ensure fairness, as emphasized in [55].

We have also emphasized in Section VI that passive physical equivalents provide a physical realization of the effective impedance, establishing an intuitive understanding of the effective impedance analysis. For instance, realizations show how a frequency dependent damping effect in the effective impedance analysis can be realized with a serial connection of an inerter with a damper, as in [50].

We have presented passive physical realizations for S(D)EA under VSIC while rendering null impedance or ideal springs in Figure 4. It is important to note that, in general, passive physical realizations for a given impedance transfer function are not unique. While the feasibility conditions for a passive physical realization provides sufficient conditions for passivity as shown in Sections IV and V, the necessary conditions may not be easily established through such analysis, as it requires studying feasibility of *all* passive physical realizations.

Figures 15a–b depict alternative passive physical realizations of SEA under VSIC during null impedance rendering when the force controller is P and the motion controller is PI. In particular, Figure 4a and Figures 15a and 15b present the realizations for the impedance transfer function in Eqn. (2). Section IV presents feasibility conditions for Figure 4a and prove that they establish a set of sufficient conditions for passivity. Figure 15a and 15b are alternative realizations, where the serial inerter-damper term introduced due to the integral controller is realized through a serial spring-damper. The feasibility conditions for these realizations provide a different set of sufficient conditions for passivity. While Bott-Duffin theorem [32] establishes that ideal transformers (levers) can be avoided in physical realizations, we present Figures 15a and 15b as a set of alternative realizations, since the feasibility conditions of these two realizations complement each other to recover the necessary and sufficient conditions for the passivity of Eqn. (2) and the use of a lever to change direction provides an understanding on how negative values of fundamental elements (e.g.,  $k_{1n}$  and  $c_{4n}$ ) can be avoided in feasible realizations.

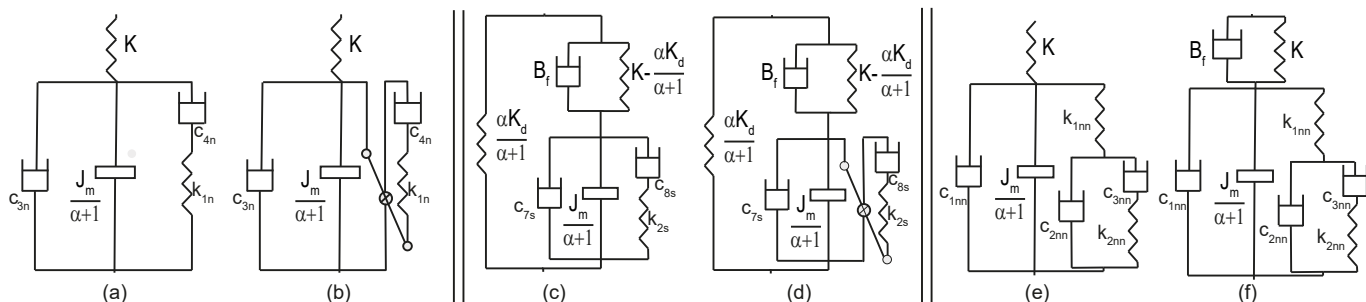


Fig. 15: (a)-(b) Alternative passive physical equivalents of SEA under VSIC during null impedance rendering when the force controller is P and the motion controller is PI, (c)-(d) Alternative passive physical equivalents of SDEA under VSIC during spring rendering when both controllers are P, and (e)-(f) Realization of S(D)EA under VSIC during null impedance rendering when both controllers are PI.

Similarly, Figures 15c–d depict alternative passive physical equivalents for the impedance in Eqn. (15) for SDEA under VSIC during spring rendering when both controllers are P. Here, Figures 15c and 15d complement each other to provide the same sufficient conditions as presented for Figure 4h.

Realizations become more complicated as controllers become more involved, making their interpretation harder. For instance, Figures 15e–f present passive physical realizations for SEA and SDEA under VSIC during null impedance rendering, when both controllers are PI.

Our ongoing work include the extension of the passivity analysis and passive realization results to S(D)EA under different controllers, such as MRFC as proposed in [23] and disturbance observer based control as proposed in [67]. We also plan to extend passive realizations to fractional-order LTI systems [52], [53], as the interpretation of these controllers can benefit from physical intuition.

This study utilizes classical frequency domain analysis techniques to derive closed-form analytical solutions for the passivity bounds of LTI systems. There exists alternative approaches for passivity analysis, for instance utilizing state-space techniques, for which several equivalences with the frequency domain analysis have been established [56]. Moreover, less conservative analysis techniques, such as time domain passivity [68] or complementary stability [54], [55], [69] can be applied, if numerical approaches are to be utilized.

As part of our future work, we plan to study extensions of the current results to S(D)EA systems that include nonlinear energy storage and dissipation elements, utilizing well-established passivity definitions and analysis techniques for nonlinear systems [70]–[72].

#### ACKNOWLEDGMENTS

This work has been partially supported under TÜBİTAK Grant 216M200.

#### REFERENCES

- [1] N. Hogan, "Impedance control: An approach to manipulation: Part I—Theory," *Journal of Dynamic Systems, Measurement, and Control*, vol. 107, no. 1, pp. 1–7, 1985.
- [2] J. E. Colgate and N. Hogan, "Robust control of dynamically interacting systems," *International Journal of Control*, vol. 48, no. 1, pp. 65–88, 1988.
- [3] R. D. Howard, "Joint and actuator design for enhanced stability in robotic force control," Ph.D. dissertation, MIT, 1990.
- [4] G. A. Pratt and M. M. Williamson, "Series elastic actuators," in *IEEE/RSJ International Conference on Intelligent Robots and Systems*, vol. 1, 1995, pp. 399–406.
- [5] D. W. Robinson, J. E. Pratt, D. J. Paluska, and G. A. Pratt, "Series elastic actuator development for a biomimetic walking robot," in *IEEE/ASME International Conference on Advanced Intelligent Mechatronics*, 1999, pp. 561–568.
- [6] C. An and J. Hollerbach, "Dynamic stability issues in force control of manipulators," in *IEEE International Conference on Robotics and Automation*, vol. 4, 1987, pp. 890–896.
- [7] S. Eppinger and W. Seering, "Understanding bandwidth limitations in robot force control," in *IEEE International Conference on Robotics and Automation*, vol. 4, 1987, pp. 904–909.
- [8] W. S. Newman, "Stability and performance limits of interaction controllers," *Journal of Dynamic Systems, Measurement, and Control*, vol. 114, no. 4, pp. 563–570, 1992.
- [9] J. Hurst, A. Rizzi, and D. Hobbelen, "Series elastic actuation: Potential and pitfalls," in *International Conference on Climbing and Walking Robots*, 2004.
- [10] J. Oblak and Z. Matjačić, "Design of a series visco-elastic actuator for multi-purpose rehabilitation haptic device," *Journal of Neuroengineering and Rehabilitation*, vol. 8, no. 1, pp. 1–14, 2011.
- [11] E. Garcia, J. C. Arevalo, G. Muñoz, and P. Gonzalez-de Santos, "Combining series elastic actuation and magneto-rheological damping for the control of agile locomotion," *Robotics and Autonomous Systems*, vol. 59, no. 10, pp. 827–839, 2011.
- [12] M. Laffranchi, N. Tsagarakis, and D. G. Caldwell, "A compact compliant actuator (compact) with variable physical damping," in *IEEE International Conference on Robotics and Automation*, 2011, pp. 4644–4650.
- [13] M. J. Kim, A. Werner, F. C. Loeffl, and C. Ott, "Enhancing joint torque control of series elastic actuators with physical damping," in *IEEE International Conference on Robotics and Automation*, 2017, pp. 1227–1234.
- [14] G. Pratt, P. Willisson, C. Bolton, and A. Hofman, "Late motor processing in low-impedance robots: impedance control of series-elastic actuators," in *American Control Conference*, 2004, pp. 3245–3251.
- [15] G. Wyeth, "Control issues for velocity sourced series elastic actuators," in *Australasian Conference on Robotics and Automation*, 2006, pp. 1–6.
- [16] —, "Demonstrating the safety and performance of a velocity sourced series elastic actuator," in *IEEE International Conference on Robotics and Automation*, 2008, pp. 3642–3647.
- [17] H. Vallery, R. Ekkelenkamp, H. Van Der Kooij, and M. Buss, "Passive and accurate torque control of series elastic actuators," in *IEEE/RSJ International Conference on Intelligent Robots and Systems*, 2007, pp. 3534–3538.
- [18] H. Vallery, J. Veneman, E. Van Asseldonk, R. Ekkelenkamp, M. Buss, and H. Van Der Kooij, "Compliant actuation of rehabilitation robots," *IEEE Robotics and Automation Magazine*, vol. 15, no. 3, pp. 60–69, 2008.
- [19] N. L. Tagliamonte and D. Accoto, "Passivity constraints for the impedance control of series elastic actuators," *Institution of Mechanical Engineers, Part I: Journal of Systems and Control Engineering*, vol. 228, no. 3, pp. 138–153, 2014.
- [20] A. Calanca, R. Muradore, and P. Fiorini, "Impedance control of series elastic actuators: Passivity and acceleration-based control," *Mechatronics*, vol. 47, pp. 37–48, 2017.
- [21] F. E. Tosun and V. Patoglu, "Necessary and sufficient conditions for the passivity of impedance rendering with velocity-sourced series elastic actuation," *IEEE Transactions on Robotics*, vol. 36, no. 3, pp. 757–772, 2020.
- [22] A. Otaran, O. Tokatli, and V. Patoglu, "Physical human-robot interaction using HandsOn-SEA: An educational robotic platform with series elastic actuation," *IEEE Transactions on Haptics*, vol. 14, no. 4, pp. 922–929, 2021.
- [23] C. U. Kenanoglu and V. Patoglu, "Passivity of series elastic actuation under model reference force control during null impedance rendering," *IEEE Transactions on Haptics*, vol. 15, no. 1, pp. 51–56, 2022.
- [24] M. Focchi, G. A. Medrano-Cerda, T. Boaventura, M. Frigerio, C. Semini, J. Buchli, and D. G. Caldwell, "Robot impedance control and passivity analysis with inner torque and velocity feedback loops," *Control Theory and Technology*, vol. 14, no. 2, pp. 97–112, 2016.
- [25] U. Mengilli, U. Caliskan, Z. O. Orhan, and V. Patoglu, "Two-port analysis of stability and transparency in series damped elastic actuation," *CoRR*, 2020. [Online]. Available: <https://arxiv.org/abs/2011.00664>
- [26] U. Mengilli, Z. O. Orhan, U. Caliskan, and V. Patoglu, "Passivity of series damped elastic actuation under velocity-sourced impedance control," in *IEEE World Haptics Conference*, 2021, pp. 379–384.
- [27] E. Colgate and N. Hogan, "An analysis of contact instability in terms of passive physical equivalents," in *International Conference on Robotics and Automation*, vol. 1, 1989, pp. 404–409.
- [28] M. C. Smith, "Synthesis of mechanical networks: the inerter," *IEEE Transactions on Automatic Control*, vol. 47, no. 10, pp. 1648–1662, 2002.
- [29] M. Z. Chen, C. Papageorgiou, F. Scheibe, F.-c. Wang, and M. C. Smith, "The missing mechanical circuit element," *IEEE Circuits and Systems Magazine*, vol. 9, no. 1, pp. 10–26, 2009.
- [30] R. M. Foster, "A reactance theorem," *Bell System Technical Journal*, vol. 3, no. 2, pp. 259–267, 1924.
- [31] O. Brune, "Synthesis of a finite two-terminal network whose driving-point impedance is a prescribed function of frequency," Ph.D. dissertation, MIT, 1931.
- [32] R. Bott and R. Duffin, "Impedance synthesis without use of transformers," *Journal of Applied Physics*, vol. 20, no. 8, pp. 816–816, 1949.

- [33] M. Z. Chen and M. C. Smith, "Mechanical networks comprising one damper and one inerter," in *IEEE European Control Conference*, 2007, pp. 4917–4924.
- [34] —, "Restricted complexity network realizations for passive mechanical control," *IEEE Transactions on Automatic Control*, vol. 54, no. 10, pp. 2290–2301, 2009.
- [35] M. Z. Chen, K. Wang, Y. Zou, and J. Lam, "Realization of a special class of admittances with one damper and one inerter," in *IEEE Conference on Decision and Control*, 2012, pp. 3845–3850.
- [36] —, "Realization of a special class of admittances with one damper and one inerter for mechanical control," *IEEE Transactions on Automatic Control*, vol. 58, no. 7, pp. 1841–1846, 2013.
- [37] M. Z. Chen, K. Wang, Z. Shu, and C. Li, "Realizations of a special class of admittances with strictly lower complexity than canonical forms," *IEEE Transactions on Circuits and Systems I*, vol. 60, no. 9, pp. 2465–2473, 2013.
- [38] M. Z. Chen, K. Wang, Y. Zou, and G. Chen, "Realization of three-port spring networks with inerter for effective mechanical control," *IEEE Transactions on Automatic Control*, vol. 60, no. 10, pp. 2722–2727, 2015.
- [39] R. Kalman, *Perspectives in Mathematical System Theory, Control, and Signal Processing*. Berlin, Heidelberg: Springer, 2010, vol. 398, ch. Old and new directions of research in system theory, p. 3.
- [40] J. Z. Jiang and M. C. Smith, "Regular positive-real functions and five-element network synthesis for electrical and mechanical networks," *IEEE Transactions on Automatic Control*, vol. 56, no. 6, pp. 1275–1290, 2011.
- [41] —, "Series-parallel six-element synthesis of biquadratic impedances," *IEEE Transactions on Circuits and Systems I*, vol. 59, no. 11, pp. 2543–2554, 2012.
- [42] T. H. Hughes and M. C. Smith, "On the minimality and uniqueness of the bott–duffin realization procedure," *IEEE Transactions on Automatic Control*, vol. 59, no. 7, pp. 1858–1873, 2014.
- [43] T. H. Hughes, "Why rlc realizations of certain impedances need many more energy storage elements than expected," *IEEE Transactions on Automatic Control*, vol. 62, no. 9, pp. 4333–4346, 2017.
- [44] —, "Minimal series-parallel network realizations of bicubic impedances," *IEEE Transactions on Automatic Control*, vol. 65, no. 12, pp. 4997–5011, 2020.
- [45] A. Morelli and M. C. Smith, *Passive Network Synthesis: An Approach to Classification*. SIAM, 2019.
- [46] S. M. Hughes T.H., Morelli A., *Electrical Network Synthesis: A Survey of Recent Work*, ser. Lecture Notes in Control and Information Sciences. Springer, 2018, ch. Emerging Applications of Control and Systems Theory, pp. 281–293.
- [47] B. Hannaford, "A design framework for teleoperators with kinesthetic feedback," *IEEE Transactions on Robotics and Automation*, vol. 5, no. 4, pp. 426–434, 1989.
- [48] K. Hashtrudi-Zaad and S. E. Salcudean, "Analysis of control architectures for teleoperation systems with impedance/admittance master and slave manipulators," *International Journal of Robotics Research*, vol. 20, no. 6, pp. 419–445, 2001.
- [49] J. Colgate and J. Brown, "Factors affecting the Z-width of a haptic display," in *IEEE International Conference on Robotics and Automation*, 1994, pp. 3205–3210.
- [50] J. S. Mehling, J. E. Colgate, and M. A. Peshkin, "Increasing the impedance range of a haptic display by adding electrical damping," in *IEEE World Haptics Conference*, 2005, pp. 257–262.
- [51] N. Colonnese, A. F. Siu, C. M. Abbott, and A. M. Okamura, "Rendered and characterized closed-loop accuracy of impedance-type haptic displays," *IEEE Transactions on Haptics*, vol. 8, no. 4, pp. 434–446, 2015.
- [52] O. Tokatli and V. Patoglu, "Stability of haptic systems with fractional order controllers," in *IEEE/RSJ International Conference on Intelligent Robots and Systems*, 2015, pp. 1172–1177.
- [53] —, "Using fractional order elements for haptic rendering," *Springer Advanced Robotics Robotics Research*, pp. 373–388, 2018.
- [54] Y. Aydin, O. Tokatli, V. Patoglu, and C. Basdogan, "Stable physical human-robot interaction using fractional order admittance control," *IEEE Transactions on Haptics*, vol. 11, no. 3, pp. 464–475, 2018.
- [55] —, "A computational multicriteria optimization approach to controller design for physical human-robot interaction," *IEEE Transactions on Robotics*, vol. 36, no. 6, pp. 1791–1804, 2020.
- [56] N. Kottenstette and P. J. Antsaklis, "Time domain and frequency domain conditions for passivity," ISIS Lab University of Notre Dame, Technical report ISIS-2008-002, 2008.
- [57] S. Haykin, *Active network theory*. Addison-Wesley Pub. Co., 1970.
- [58] F. F. Kuo, *Network Analysis and Synthesis*. John Wiley and Sons, 1962.
- [59] C. U. Kenanoglu and V. Patoglu, "Supplementary document for passive realizations of series elastic actuation," Sabanci University, Tech. Rep., 2022. [Online]. Available: <https://tinyurl.com/bdz3mckt>
- [60] A. Kamadan, G. Kiziltas, and V. Patoglu, "Co-design strategies for optimal variable stiffness actuation," *IEEE/ASME Transactions on Mechatronics*, vol. 22, no. 6, pp. 2768–2779, 2017.
- [61] —, "A systematic design selection methodology for system-optimal compliant actuation," *Robotica*, vol. 37, no. 4, pp. 656–674, 2019.
- [62] U. Caliskan, A. Apaydin, A. Otaran, and V. Patoglu, "A series elastic brake pedal to preserve conventional pedal feel under regenerative braking," in *IEEE/RSJ International Conference on Intelligent Robots and Systems*, 2018, pp. 1367–1373.
- [63] U. Caliskan and V. Patoglu, "Efficacy of haptic pedal feel compensation on driving with regenerative braking," *IEEE Transactions on Haptics*, vol. 13, no. 1, pp. 175–182, 2020.
- [64] T. K. Ghaffari and J. Kövecses, "A high-performance velocity estimator for haptic applications," in *IEEE World Haptics Conference*, 2013, pp. 127–132.
- [65] J. E. Colgate, "The control of dynamically interacting systems," Ph.D. dissertation, MIT, 1988.
- [66] D. P. Losey and M. K. O'Malley, "Effects of discretization on the k-width of series elastic actuators," in *IEEE International Conference on Robotics and Automation*, 2017, pp. 421–426.
- [67] K. Kong, J. Bae, and M. Tomizuka, "Control of rotary series elastic actuator for ideal force-mode actuation in human-robot interaction applications," *IEEE/ASME Transactions on Mechatronics*, vol. 14, no. 1, pp. 105–118, 2009.
- [68] B. Hannaford and J.-H. Ryu, "Time domain passivity control of haptic interfaces," *IEEE Transactions on Robotics and Automation*, vol. 18, no. 1, pp. 1–10, 2002.
- [69] S. P. Buerger and N. Hogan, "Complementary stability and loop shaping for improved human-robot interaction," *IEEE Transactions on Robotics*, vol. 23, no. 2, pp. 232–244, 2007.
- [70] R. Ortega, J. A. L. Perez, P. J. Nicklasson, and H. J. Sira-Ramirez, *Passivity-based control of Euler-Lagrange systems: mechanical, electrical and electromechanical applications*. Springer Science and Business Media, 2013.
- [71] V. Duindam, A. Macchelli, S. Stramigioli, and H. Bruyninckx, *Modeling and control of complex physical systems: the port-Hamiltonian approach*. Springer Science and Business Media, 2009.
- [72] A. Van Der Schaft, D. Jeltsema et al., "Port-Hamiltonian systems theory: An introductory overview," *Foundations and Trends in Systems and Control*, vol. 1, no. 2-3, pp. 173–378, 2014.

**Celal Umut Kenanoglu** received his B.Sc. degree in mechanical engineering from Izmir Institute of Technology (2019) and his M.Sc. in mechatronics engineering from Sabanci University (2022). Currently, he is pursuing his Ph.D. in Munich Institute of Robotics and Machine Intelligence at Technical University of Munich. His research interests include interaction control, physical human-robot interaction, and haptic rendering.



**Volkan Patoglu** is a professor in mechatronics engineering at Sabanci University. He received his Ph.D. degree in mechanical engineering from the University of Michigan, Ann Arbor (2005) and worked as a post doctoral research associate at Rice University (2006). His research is in the area of physical human-machine interaction, in particular, design and control of force feedback robotic systems with applications to rehabilitation. His research extends to cognitive robotics. Dr. Patoglu has served as an associate editor for IEEE Transactions on Haptics



(2013–2017) and is currently an associate editor for IEEE Transactions on Neural Systems and Rehabilitation Engineering, and IEEE Robotics and Automation Letters.